group (odds ratio 3.2, 95% CI 1.01–10.3; P = .04), but other structural heart diseases showed no significant difference between the two cohort groups. Of note, the prevalence of both hypertension and valvular heart disease was significantly higher in the AF group (4/15 [26.7%]) than in the non-AF group (3/63 [4.8%]; odds ratio 7.3, 95% CI 1.4–37.1; P = .018).

Characteristics of ECG

ECG characteristics are listed in Table 3. No significant difference with regard to heart rate and frontal plane P-wave axis was seen between the AF and non-AF groups. The total duration of P wave in lead V_1 was significantly longer in the AF group than in the non-AF group. In contrast, the total amplitude (amplitude from top to bottom level) of the P wave in lead V_1 was not significant between the two groups.

For the two cohorts, we first evaluated the P-wave terminal portion in lead V_1, which was assigned as a marker for choosing patients from the database in the study. Table 4 (top) lists measurements of the P-wave terminal portion in lead V_1. The area of the P-wave terminal portion did not differ between the AF and non-AF groups. Neither the duration nor the amplitude of the P-wave terminal portion was different between the AF and non-AF groups. The same was true for the P-wave terminal force between the two groups. Because no significant difference in P-wave terminal portion in lead V_1 was observed between the AF and non-AF groups, we then estimated the initial portion of P wave in lead V_1. Table 4 (bottom) lists measurements of the P-wave initial portion in lead V_1. The area of the P-wave initial portion was significantly larger in the AF group than in the non-AF group. The duration of the P-wave initial portion was significantly longer in the AF group than in the non-AF group, and the amplitude of the P-wave initial portion was significantly higher in the AF group than in the non-AF group. Therefore, the P-wave initial force was significantly greater in the AF group than in the non-AF group.

AF development

Based on the significant association of the P-wave initial portion in lead V_1 with AF development, the AF-free event rate was estimated according to the area of P-wave initial portion. Using receiver operating characteristic analysis, the sensitivity and specificity of P-wave initial portion in response to developing AF were maximized by the area of P-wave initial portion of 65 (relative risk 4.0, 95% CI 1.2–13.1). Kaplan-Meier life-table analysis is shown in Figure 3. The area of the P-wave initial portion was associated with a significant difference of AF-free event rate between patients with area of P-wave initial portion ≥65 (n = 39) and those with area of P-wave initial portion <65 (n = 39; hazard ratio 4.02, 95% CI 1.25–17.8; P = .02). The rate of use of Class I antiarrhythmic drugs was identical between patients with area of P-wave initial portion ≥65 and those with area of P-wave initial portion <65 (10% vs 8%; P = .72). Because age is an important factor affecting the development of AF, the AF-free event rate was compared between patients <65 years old (n = 55) and those ≥65 years (n = 23). No significant difference was seen with regard to age (hazard ratio age ≥65 years to age <65 years = 2.39, 95% CI 0.72–7.19; P = .12). The AF-free event rate between patients with and those without hypertension was compared because hypertension was more prevalent in the AF group than in the non-AF group, but the presence of hypertension did not significantly affect the development of AF (hazard ratio of presence to absence of hypertension = 1.4, 95% CI 0.4–4.4; P = .54). In addition, no significant gender difference was found with regard to the AF-free

Table 3 Characteristics of ECG

Measurement	AF group	Non-AF group	P value
Heart rate (bpm)	69.0 ± 22.4	84.1 ± 19.3	.99
P-wave axis (°)	60.5 ± 20.5	61.9 ± 14.3	.62
P wave (ms) in lead V_1			
Total duration (ms)	126.7 ± 14.8	115.8 ± 16.7	.012
Total amplitude (μV)	310.7 ± 15.8	302.9 ± 64.9	.33

Table 4 Measurements of P wave in lead V_1

Measurement	AF group	Non-AF group	P value
Terminal Portion			
Duration (ms)	84.5 ± 15.0	80.1 ± 12.5	.123
Amplitude (μV)	−216.7 ± 20.1	−234.0 ± 40.0	.108
Area (μV × ms)	468.2 ± 155.0	477.7 ± 139.5	.41
Terminal force (s × μV)	18,491 ± 5,149	18,779 ± 4,584	.42
Initial Portion			
Duration (ms)	42.2 ± 12.4	35.7 ± 10.1	.018
Amplitude (μV)	94.0 ± 39.9	68.8 ± 49.4	.035
Area (μV × ms)	114.6 ± 73.0	73.1 ± 59.3	.011
Initial force (s × μV)	4,346.7 ± 2,712	2,650.3 ± 2,375	.0089

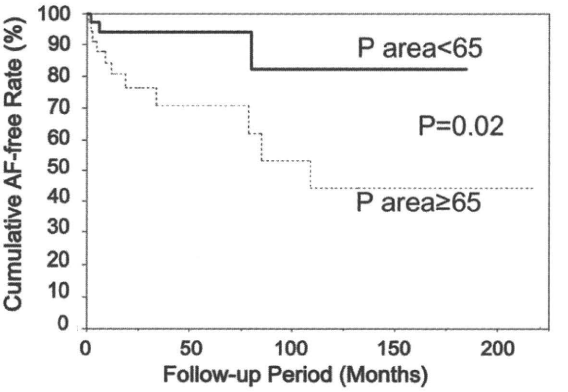

Figure 3 Kaplan-Meier estimates of atrial fibrillation (AF)-free event rate in patients with left atrial overload according to the area of P-wave initial portion in lead V_1. The AF-free event rate in patients with area of P-wave initial portion ≥65 μV × ms was significantly lower than in those with area of P-wave initial portion <65 μV × ms (P = .02).

Table 5 Probability of AF development during follow-up based on clinical and ECG variables

	Hazard ratio	95% Confidence interval	*P* value
P area ≥65 μV × ms	4.07	1.16–19.4	.02
P area <65 μV × ms	1	—	—
Age ≥65 years	1.96	0.56–6.18	.28
Age <65 years	1	—	—
Hypertension	0.91	0.27–3.09	.87
No hypertension	1	—	—
Male	0.79	0.23–2.88	.71
Female	1	—	—

AF = atrial fibrillation; ECG = electrocardiographic.

event rate (hazard ratio of male to female 1.0, 95% CI 0.3–3.3; $P = .99$).

Multivariate analysis confirmed that the area of P-wave initial portion was independently associated with an increased propensity for development of AF (Table 5). After adjustment for age and gender, the hazard ratio for AF development was 4.07 (95% CI 1.16–19.4; $P = .02$). The level of the area of P-wave initial portion in lead V_1 was compared in patients with and those without hypertension. The area of P-wave initial portion in lead V_1 was not significantly different between patients with and those without hypertension (84 ± 59 vs 80 ± 67, respectively; $P = .80$) and was not significantly different between patients ≥65 years old and those <65 years (86 ± 67 vs 79 ± 62; $P = .69$). In addition, gender was not significantly related to the area of P-wave initial portion (male 83 ± 61, female 77 ± 70; $P = .68$), nor was left ventricular ejection fraction ($R^2 = 0.00048$, $P = .86$ by linear regression analysis).

Discussion

Since the early description of an asynchrony of atrial depolarization by Reynolds,[12] several studies reported P-wave abnormality suggesting LA enlargement.[13–15] In 1964, Morris et al[3] advanced this concept as representing LA overload. They proposed that P terminal force >0.04 second in duration and >0.1 mV in depth at lead V_1 was associated with hemodynamically strained LA in various valvular heart diseases. Since then, increased P terminal force in lead V_1 has been considered a probable precursor to development of AF, as patients with such disorders likely suffer from AF. In this study, we systematically tested in a large size of population the hypothesis that P wave with LA overload is linked to the development of AF. Consistent with previous epidemiologic studies,[16,17] AF occurred in a few percentage of control patients in this study but occurred at a substantially higher incidence in AF patients with LA overload. Our results confirmed that when LA overload was present, the magnitude of overload in the RA could be independently attributed to the development of AF, indicating that analysis of P wave in lead V_1 deserves consideration for predicting AF. This is an important for clinicians. The measurements of P wave in our study were performed using 12-lead ECG recordings, which are commonly available in clinical practice. Moreover, computer-based measurements were performed at high resolution for data analysis of P-wave variables, which provides precise reproducibility.

P wave and AF

A principal aim of this study was to establish the prognostic importance of the P wave in lead V_1. The terminal portion of the P wave in lead V_1 has been associated with electrical depolarization of the LA alone in humans[18] and in dogs.[19] Using angiocardiography, Miller and Spertus[20] showed a correlation of marked negative component in leads V_1 and V_2 with LA enlargement. Subsequently, Morris et al[3] showed a significant correlation of the magnitude of P terminal force with severity of hemodynamic abnormality. The P terminal portion in lead V_1 is composed of several factors: (1) anatomic shift of the LA to the posterior side by hemodynamic strain, (2) enlarged LA size, (3) LA hypertrophy, and (4) reduced conduction velocity in the LA.[8,21,22] These factors are also attributed to prolonged P-wave duration. We used a much larger P terminal force for patient selection in this study than did Morris et al. Therefore, it is reasonable to speculate that patients included in this study have a high probability of AF occurrence. Indeed, compatible with this assumption, patients with marked LA overload developed AF at a substantially higher rate than did control patients. This finding indicates that increased magnitude of P-wave terminal portion in lead V_1 is a useful marker for predicting the development of AF. Furthermore, in the current study, the increased P-wave terminal portion provided information on predictivity of AF when the P-wave initial portion in lead V_1 was additively estimated. Regardless of the magnitude of the P-wave terminal portion in lead V_1, however, the magnitude of the P-wave initial portion in lead V_1 was attributed to the development of AF. This finding indicates that overload in the RA may be critical to the development of AF, and atrial vulnerability to fibrillation is likely to increase when both atria are overloaded. In addition to LA overload, electrophysiologic abnormality in the RA may increase susceptibility to AF development. Although depolarization originating from the atrial septum and/or left atrium may participate in part of the P-wave initial portion, the P-wave initial portion in lead V_1 mainly represents depolarization of the RA. Thus, our data indicate the importance of evaluating whether or not the RA is overloaded when LA overload is present. Although Class I antiarrhythmic drugs were used more frequently in the AF group than in the non-AF group, the drugs were administered similarly between two groups dichotomized according to the area of P-wave initial portion, thereby indicating that overload in the RA is an independent prognostic marker of AF.

P-wave features observed in this study reflect electrophysiologic and structural remodeling of the atrium that predisposes to the development of AF. Increased P-wave duration results from either slow conduction or an enlarged atrium. The former shortens wavelength, and the latter provides a sufficient area for reentry to occur. These pathophysiologic changes are linked to the maintenance of AF.[6]

Increased intracardiac pressure of the left ventricle may cause LA remodeling, which is likely to occur in patients with structural heart disease. Disturbed transmitral blood flow due to elevated diastolic pressure in the left ventricle may induce heterogeneous distribution of the atrial refractory period. Structural remodeling, as occurs with interstitial fibrosis and connexin redistribution, causes anisotropic conduction or discontinuous propagation. In hypertrophied atrial myocytes, triggered activity, such as early and delayed afterdepolarizations, is prone to occur.[23,24] The present study showed that an increased magnitude of P-wave initial force in lead V_1 was associated with a higher rate of AF development. This finding suggests that when a substrate develops in the RA in addition to the LA, susceptibility to the development of AF may increase.

Study limitations

Because the retrospective cohort study was conducted using ECGs recorded in our hospital, several limitations are inherent. First, we determined AF development by reviewing past ECGs, but recordings of AF might have been missed if AF terminated spontaneously before the ECGs were recorded in the hospital. Because no AF can be documented during follow-up of a patient who suffered from transient AF, this patient was classified into the non-AF group, and the AF-free duration appears longer than the true AF-free duration. Second, in the present study, LA overload was defined based on the P-wave terminal portion in lead V_1. Although this ECG marker is representative of LA overload, surrounding tissue of the heart (e.g., fat and lung) may affect the amplitude and area of the P-wave terminal portion in lead V_1, indicating that how precisely the P-wave terminal portion reflected LA overload might differ depending on the individual. Third, because our study included patients who underwent ECG recording in our hospital, the risk of AF in the study population undoubtedly was greater than that in the general population. Therefore, this factor should be considered when our results are extrapolated to a broader population.

Clinical implications

AF is one of the most common cardiac rhythm disorders; however, useful ECG identification of patients at greatest risk for developing AF remains the preeminent challenge to physicians who care for AF-prone patients. Assessment of signal-averaged ECGs of P wave has served as the principal noninvasive means of determining AF risk. This method, which estimates vulnerability to AF, is fundamentally based on delayed conduction, which may provide the substrate for reentry. Consistent with signal-averaged ECG, our ECG parameters also reflect interatrial conduction disturbance. Our data indicate that P-wave analysis using standard 12-lead ECG recordings could successfully detect a risk stratifier of AF. In addition, our quantitative relationship between P wave and vulnerability to AF could be exploited to define the risk of AF development and determine which patients are most likely to benefit from preventive anticoagulant therapy. Our results suggest that coexistence of overload in the RA and the LA may be useful for evaluating some patients. For example, screening patients with palpitations might provide a means for identifying those at high risk for AF development. In order to make measurement of the P wave a widely available marker for patients, improvements of the automatic algorithm for analysis of 12-lead ECGs are needed to predict AF in a timely fashion.

Acknowledgements

We thank Kahaku Emoto, Seiichi Fujisaki, and Tatsumi Uchiyama (GE Yokokawa Medical System Co.) for technical assistance.

References

1. Abildskov JA, Cronvich JA, Burch GE. An analysis of activation in human atria. Circulation 1955;11:97–105.
2. Haywood LJ, Selvester RH. Analysis of right and left atrial vectorcardiograms. Timed records of 100 normal persons. Circulation 1966;33:577–587.
3. Morris JJ Jr, Estes EH Jr, Whalen RE, Thompson HK Jr, McIntosh HD. P-wave analysis in valvular heart disease. Circulation 1964;29:242–252.
4. Munuswamy K, Alpert MA, Martin RH, Whiting RB, Mechlin NJ. Sensitivity and specificity of commonly used electrocardiographic criteria for left atrial enlargement determined by M-mode echocardiography. Am J Cardiol 1984;53:829–832.
5. Hazen MS, Marwick TH, Underwood DA. Diagnostic accuracy of the resting electrocardiogram in detection and estimation of left atrial enlargement: an echocardiographic correlation in 551 patients. Am Heart J 1991;122:823–828.
6. Allessie M, Ausma J, Schotten U. Electrical, contractile and structural remodeling during atrial fibrillation. Cardiovasc Res 2002;54:230–246.
7. Shettigar UR, Barry WH, Hultgren HN. P wave analysis in ischaemic heart disease. An echocardiographic, haemodynamic, and angiographic assessment. Br Heart J 1977;39:894–899.
8. Josephson ME, Kastor JA, Morganroth J. Electrocardiographic left atrial enlargement. Electrophysiologic, echocardiographic and hemodynamic correlates. Am J Cardiol 1977;39:967–971.
9. Ciaroni S, Cuenoud L, Bloch A. Clinical study to investigate the predictive parameters for the onset of atrial fibrillation in patients with essential hypertension. Am Heart J 2000;139:814–819.
10. De BD, Willekens J, De BG. Long-term prognostic value of p-wave characteristics for the development of atrial fibrillation in subjects aged 55 to 74 years at baseline. Am J Cardiol 2007;100:850–854.
11. Guidera SA, Steinberg JS. The signal-averaged P wave duration: a rapid and noninvasive marker of risk of atrial fibrillation. J Am Coll Cardiol 1993;21:1645–1651.
12. Reynolds G. The atrial electrogram in mitral stenosis. Br Heart J 1953;15:250–258.
13. Martines DE Oliv, Zimmerman HA. Auricular overloadings: electrocardiographic analysis of 193 cases. Am J Cardiol 1959;3:453–471.
14. Soloff LA, Zatuchni J. Relationship of the P wave to left atrial volume in rheumatic heart disease with mitral stenosis. Am J Med Sci 1958;235:290–296.
15. Revalo AC, Spagnuolo M, Feinstein AR. A simple electrocardiographic indication of left atrial enlargement. A study of young patients with rheumatic heart disease. JAMA 1963;185:358–362.
16. Feinberg WM, Blackshear JL, Laupacis A, Kronmal R, Hart RG. Prevalence, age distribution, and gender of patients with atrial fibrillation. Analysis and implications. Arch Intern Med 1995;155:469–473.
17. Tanizaki Y, Kiyohara Y, Kato I, et al. Incidence and risk factors for subtypes of cerebral infarction in a general population: the Hisayama study. Stroke 2000; 31:2616–2622.
18. Wenger R, Hofmann-Credner D. Observations on the atria of the human heart by direct and semidirect electrocardiography. Circulation 1952;5:870–877.
19. Puech P, Esclavissat M, Sodi-Pallares D, Cisneros F. Normal auricular activation in the dog's heart. Am Heart J 1954;47:174–191.
20. Miller HI, Spertus I. P wave changes reflecting atrial morphology. Dis Chest 1964;46:578–591.
21. Sutnick AI, Soloff LA. Posterior rotation of the atrial vector. An electrocardiographic sign of left ventricular failure. Circulation 1962;26:913–916.
22. Gooch AS, Calatayud JB, Gorman PA, Saunders JL, Caceres CA. Leftward shift of the terminal P forces in the ECG associated with left atrial enlargement. Am Heart J 1966;71:727–733.
23. Benjamin EJ, Chen PS, Bild DE, et al. Prevention of atrial fibrillation: report from a national heart, lung, and blood institute workshop. Circulation 2009;119: 606–618.
24. Nattel S. New ideas about atrial fibrillation 50 years on. Nature 2002;415:219–226.

High prevalence of early repolarization in short QT syndrome

Hiroshi Watanabe, MD, PhD, FESC,* Takeru Makiyama, MD, PhD,† Taku Koyama, MD,‡ Prince J. Kannankeril, MD, MSCI,¶ Shinji Seto, MD,§ Kazuki Okamura, MD, PhD,‖ Hirotaka Oda, MD, PhD,‖ Hideki Itoh, MD, PhD,** Masahiko Okada, MD, PhD,†† Naohito Tanabe, MD, PhD,‡‡ Nobue Yagihara, MD,* Shiro Kamakura, MD, PhD,‡ Minoru Horie, MD, PhD,** Yoshifusa Aizawa, MD, PhD,* Wataru Shimizu, MD, PhD‡

*From the *Division of Cardiology, Niigata University Graduate School of Medical and Dental Sciences, Niigata, Japan, †Department of Cardiovascular Medicine, Kyoto University Graduate School of Medicine, Kyoto, Japan, ‡Division of Cardiology, Department of Internal Medicine, National Cardiovascular Center, Suita, Japan, ¶Department of Pediatrics, Vanderbilt University School of Medicine, Nashville, Tennessee, §Department of Cardiology, Inoue Hospital, Nagasaki, Japan, ‖Department of Cardiology, Niigata City General Hospital, Niigata, Japan, **Department of Cardiovascular and Respiratory Medicine, Shiga University of Medical Science, Shiga, Japan, ††Department of Laboratory Medicine, Niigata University Graduate School of Medical and Dental Sciences, Niigata, Japan, and ‡‡Division of Health Promotion, Niigata University Graduate School of Medical and Dental Sciences, Niigata, Japan.*

BACKGROUND Short QT syndrome (SQTS) is characterized by an abnormally short QT interval and sudden death. Due to the limited number of cases, the characteristics of SQTS are not well understood. It has been reported recently that early repolarization is associated with idiopathic ventricular fibrillation and the QT interval is short in patients with early repolarization.

OBJECTIVE The purpose of this study was to study the association between early repolarization and arrhythmic events in SQTS.

METHODS The study consisted of three cohorts: SQTS cohort (N = 37), control cohort with short QT interval and no arrhythmic events (N = 44), and control cohort with normal QT interval (N = 185). ECG parameters were compared among the study cohorts.

RESULTS Heart rate, PR interval, and QRS duration were similar among the three study cohorts. Early repolarization was more common in the SQTS cohort (65%) than in the short QT control cohort (30%) and the normal QT control cohort (10%). Duration from T-wave peak to T-wave end was longer in the SQTS cohort than in the short QT control cohort, although QT and corrected QT intervals were similar. In the SQTS cohort, there were more males among patients with arrhythmic events than in those with a family history but without arrhythmic events. In multivariate models, early repolarization was associated with arrhythmic events in the SQTS cohort. ECG parameters including QT and QTc intervals were not associated with arrhythmic events in the SQTS cohort.

CONCLUSION There is a high prevalence of early repolarization in patients with SQTS. Early repolarization may be useful in identifying risk of cardiac events in SQTS.

KEYWORDS Arrhythmia; Electrocardiogram; QT interval; Repolarization; Sudden death

ABBREVIATIONS **QTc** = corrected QT interval; **SQTS** = short QT syndrome

(Heart Rhythm 2010;7:647–652)

Introduction

The short QT syndrome (SQTS) is characterized by an abnormally short QT interval and increased risk of ventricular fibrillation and sudden death.[1,2] Similar to other arrhythmia syndromes, such as long QT syndrome and Brugada syndrome,[3] SQTS is a genetically heterogeneous disease, and, to date, five responsible genes encoding different ion channels have been identified.[3–7] Some inherited arrhythmia syndromes may share genetic backgrounds that result in overlapping arrhythmia phenotypes.[3]

Although early repolarization is generally considered benign,[8] it has been reported recently that early repolarization is associated with increased risk for sudden cardiac death in patients with idiopathic ventricular fibrillation.[9–12] Haissaguerre et al[9] reported that, among patients with idiopathic ventricular fibrillation, the QT interval was shorter in patients with early repolarization than in those without, suggesting an association between early repolarization and QT interval shortening. Evidence that mutations in calcium channel genes are associated with Brugada-type ST-segment elevation and abnormally short QT intervals further suggests a relationship between early phase repolarization abnormalities and short QT interval.[4] Here we report on our

Drs. T. Makiyama, M. Horie, and W. Shimizu were supported in part by the Research Grant for the Cardiovascular Diseases (21C-8) from the Ministry of Health, Labour and Welfare, Japan. **Address reprint requests and correspondence:** Dr. Wataru Shimizu, Division of Cardiology, Department of Internal Medicine, National Cardiovascular Center, 5-7-1 Fujishiro-dai, Suita 565-8565, Japan. E-mail address: wshimizu@hsp.ncvc.go.jp. (Received November 29, 2009; accepted January 9, 2010.)

1547-5271/$ -see front matter doi:10.1016/j.hrthm.2010.01.012

study of the prevalence of early repolarization and its association with arrhythmic events in SQTS.

Methods

This cooperative study consisted of three cohorts. (1) *SQTS cohort* included patients with SQTS referred to our institutions and patients with SQTS from previous reports. The diagnosis of SQTS was made if a patient with a short QT interval [corrected QT interval (QTc) by Bazett formula ≤330 ms] had an arrhythmic event including documented ventricular fibrillation, resuscitated sudden cardiac death, and syncope and/or had a family history of SQTS, or if a patient with a short QT interval (QTc ≤360 ms) had mutations in ion channel genes responsible for SQTS.[3,13] We searched in the electronic databases PubMed, EMBASE, and Cochrane for all published studies that examined patients with SQTS. The search was limited to the end of June 2009. Published studies were considered eligible if they included clinical characteristics of the patients and ECGs. All ECGs from patients reported in the literature were reanalyzed. Electrophysiologic study was performed in patients with SQTS based on the indication of each institution. (2) *Control cohort with short QT interval* (QTc ≤330 ms) *and no arrhythmic events* was selected from among 86,068 consecutive ECGs stored on the ECG database at Niigata University Medical and Dental Hospital from May 7, 2003 to July 2, 2009. Subjects who did not have arrhythmic events or cardiovascular disease and were not taking any medication were included in this cohort. (3) *Control cohort with normal QT interval* was also selected from the ECG database. This cohort consisted of subjects who were matched to the SQTS cohort for gender and age. Subjects who had normal QT interval (360–440 ms) and did not have cardiovascular disease or were not taking any medication were included in this cohort. Subjects with Brugada-type ST-segment elevation were excluded from all study cohorts.[3,9]

QT intervals were measured on lead V_2 with the tangent methods for determination of QT_{end} using a semi-automated digitizing program with electronic calipers by an experienced observer blinded to the clinical details of all subjects included in this study.[14,15] Early repolarization was defined as elevation of the J point noted as either as QRS slurring or notching ≥0.1 mV in more than two leads.[9]

Differences in parameters were analyzed using multivariable logistic regression models when SQTS cohort and control cohort with short QT interval were compared and analyzed using conditional logistic regression models when SQTS cohort and control cohort with normal QT interval were compared. All statistical analyses were performed with SPSS (version 12.0, SPSS, Inc., Chicago, IL, USA). Two-sided $P < .05$ was considered significant. Values are expressed as mean ± SD. The study protocol was approved by the Ethics Committee of Niigata University School of Medicine. To determine interobserver variability, a second observer made independent blinded QT interval determinations of all study subjects with short QT interval.

Results

Thirty-seven patients with SQTS were identified: 12 from our institutions and 25 reported in the literature,[2,5,6,14,16–25] Forty-four control subjects with short QT interval and 185 control subjects with normal QT interval also were identified (Table 1). The SQTS cohort consisted of 25 (68%) patients with symptoms, including 14 with cardiac arrest (3 sudden death, 11 resuscitated) and 11 with syncope. Genetic screening identified mutations in ion channels in 7 (41%) of 17 probands who were genetically screened (2 *KCNQ1*, 4 *KCNH2*, 1 *KCNJ2*). Among patients in our institutions and those reported in the literature, there was no difference with regard to gender, age, prevalence of family history, QT or QTc interval, or inducibility of ventricular tachyarrhythmia by electrical programmed stimulation.

Heart rate, PR interval, and QRS duration in the SQTS cohort were not different among patients in either the short QT control cohort or the normal QT control cohort (Table 1). QT and corrected QT intervals were shorter in the SQTS and short QT control cohorts than in the normal QT control cohort. Early repolarization occurred in 24 (65%) patients with SQTS (Figure 1). Interobserver variability between two investigators was 8.6 ms (95% confidence interval −0.5 to 17.7 ms) for QT interval and 9.0

Table 1 ECG parameters of study cohorts

	Patients with SQTS (N = 37)	Subjects with short QTc (N = 44)	Versus subjects with short QTc*		Subjects with normal QTc† (N = 185)	Versus subjects with normal QTc	
			OR (95% CI)	*P* value		OR (95% CI)	*P* value
Male gender [N (%)]	27 (73)	34 (77)	2.84 (0.72–11.2)	.14	135 (73)	—	—
Age (years)	30 ± 19	47 ± 23	1.05 (1.02–1.08)	.001	30 ± 19	—	—
Heart rate (bpm)	69 ± 393	65 ± 398	1.00 (1.00–1.01)	.3	70 ± 327	1.00 (1.00–1.00)	0.70
PR interval (ms)	138 ± 19	153 ± 38	1.01 (0.99–1.03)	.54	143 ± 24	0.99 (0.97–1.01)	0.18
QRS interval (ms)	86 ± 7	84 ± 8	0.97 (0.91–1.04)	.38	85 ± 7	1.01 (0.96–1.06)	0.74
QT interval (ms)	286 ± 36	286 ± 15	0.99 (0.97–1.01)	.28	367 ± 36	0.97 (0.96–0.98)	<0.001
QTc (ms)	308 ± 29	299 ± 21	0.98 (0.96–1.00)	.06	399 ± 24	0.97 (0.97–0.98)	<0.001

CI = confidence interval; OR = odds ratio; QTc = corrected QT interval; SQTS = short QT syndrome.

*Models were adjusted for gender and age.

†Gender and age were matched between patients with SQTS and subjects with normal QT interval.

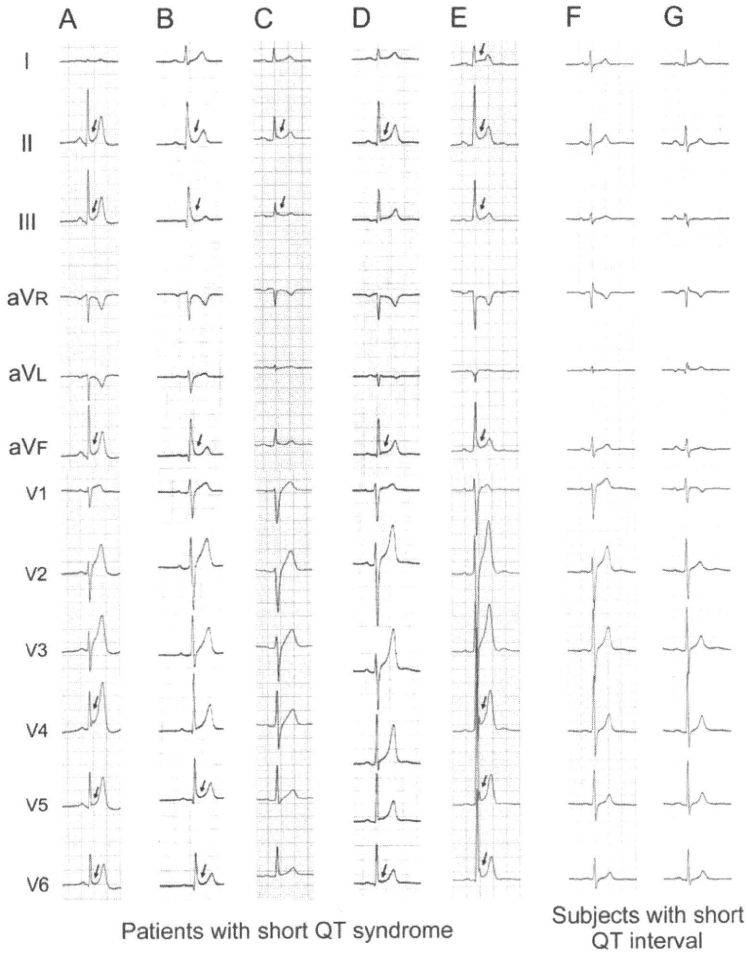

Figure 1 Early repolarization in short QT syndrome. ECGs were recorded from patients with short QT syndrome (**A:** 61-year-old woman; **B:** 30-year-old man; **C:** 38-year-old man; **D:** 31-year-old man; **E:** 22-year-old man) and control subjects with a short QT interval (**F:** 23-year-old man; **G:** 44-year-old woman). In each patient with short QT syndrome, early repolarization was evident in the inferolateral leads (*arrows*).

ms (95% confidence interval −0.6 to 18.7 ms) for QTc interval. The frequency of early repolarization was not different between patients in our institutions and those reported in the literature. Early repolarization was present in the inferior leads (II, III, aVF) in 9 patients, in the lateral leads (I, aVL, V_4–V_6) in 6 patients, and in both the inferior and lateral leads in 9 patients. Of 10 probands with early repolarization genetically screened, mutations were identified in 3 patients (1 *KCNQ1*, 2 *KCNH2*). Early repolarization was more common in the SQTS cohort than in the short QT control and normal QT control cohorts (Figure 2).

The association of early repolarization with arrhythmic events then was studied in patients with SQTS. In the SQTS cohort, there were more males among patients with arrhythmic events than among those with a family history but without arrhythmic events (Table 2). In multivariate models adjusted for gender and age, early repolarization was associated with arrhythmic events, although ECG parameters including QT and QTc intervals were not associated with arrhythmic events. Early repolarization remained associated with arrhythmic events after adjustment for age, gender, and QTc interval (P = .001). Electrophysiologic study performed in 18 patients with SQTS revealed no difference in inducibility of ventricular tachyarrhythmia between patients with arrhythmic events (73%) and those without arrhythmic events (71%).

QT interval parameters were compared between SQTS and short QT control cohorts because some of the parameters recently have been associated with SQTS.[26] Interval from T-wave peak to T-wave end (T_{peak} to T_{end}) was longer in the SQTS cohort than in the short QT control cohort even after heart rate correction using the Bazett formula, whereas QT interval, QTc interval, and interval from Q-wave to T-wave peak (QT_{peak}) were not different between the two cohorts (Table 3). Ratio of T_{peak} to T_{end} per QT was larger in the SQTS cohort than in the short QT control cohort.

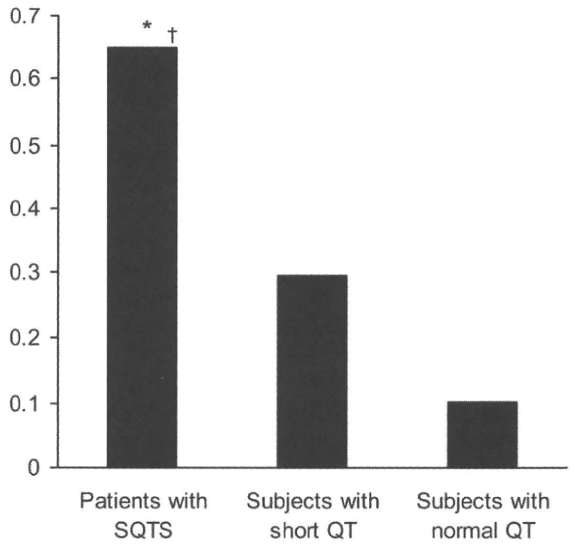

Figure 2 Frequency of early repolarization. Odds ratios (95% confidence intervals) for early repolarization in patients with short QT syndrome (SQTS) were 5.64 (1.97–16.15) and 16.58 (7.2–38.21) versus subjects with short QT interval and those with normal QT interval, respectively. *P = .001 vs subjects with short QT interval. †P <.001 vs subjects with normal QT interval.

Discussion

SQTS is a recently discovered, very rare disease with an increased risk of sudden death.[2] Due to the limited number of cases, the characteristics of SQTS are not well understood. Therefore, we conducted a cooperative analysis of ECGs from patients with SQTS in our institutions and those reported in the literature and found that early repolarization is common in SQTS.

Early repolarization is a common ECG finding. It is present in 1% to 13% of the general population and usually is considered as a normal variant due to its benign long-term prognosis.[8,11,27–29] However, increasing evidence suggests that early repolarization is associated with arrhythmia.[9,27,30–34] Since 1985, we and other investigators have reported an association between early repolarization (or late depolarization) and sudden cardiac death.[30–32] A multicenter study including our institution recently showed that early repolarization is present in one third of patients with idiopathic ventricular fibrillation.[9] Early repolarization is associated with increased risk of sudden cardiac arrest in idiopathic ventricular fibrillation, and the amplitude of early repolarization increases before development of arrhythmic events.[9,10] In Brugada syndrome, which is characterized by J-wave and ST-segment elevation in the right precordial leads on ECG and sudden cardiac death,[3] early repolarization in the inferolateral leads is not uncommon and is associated with arrhythmic events,[34] although another report has shown negative results.[33] In our study, early repolarization in the inferolateral leads was frequently found in SQTS and, more importantly, was associated with arrhythmic events in SQTS. In addition to arrhythmia syndromes unassociated with structural heart disease, a high frequency of early repolarization in arrhythmogenic right ventricular dysplasia/cardiomyopathy has been reported.[27]

It has been suggested that SQTS and idiopathic ventricular fibrillation share clinical characteristics.[23] Short QT interval is frequently found in idiopathic ventricular fibrillation,[23] and QT interval is relatively short in patients with idiopathic ventricular fibrillation who have early repolarization.[9] Spontaneous and inducible ventricular fibrillation can be initiated by short-coupled premature ventricular beat in SQTS and idiopathic ventricular fibrillation.[21,35,36] The efficacy of isoproterenol and quinidine has been reported for both arrhythmia syndromes,[21,37] although the arrhythmogenic effects of isoproterenol in an experimental model of SQTS have been reported.[38] Our study showing an association of early repolarization with SQTS further supports the presence of common arrhythmogenic substrates in SQTS and idiopathic ventricular fibrillation.

A precise mechanism for ventricular fibrillation in SQTS is not known, but characteristic ECG abnormalities may reflect arrhythmogenicity. A prior study showed that the interval from T-wave peak to T-wave end is relatively long in SQTS, and our study replicated the results.[26] T-wave peak to T-wave end interval is considered to reflect transmural dispersion of repolarization, and relative prolongation of the interval in SQTS may indicate a high vulnerability to ventricular fibrillation.[39] An experimental model of SQTS

Table 2 Characteristics of SQTS patients with and those without arrhythmic events

	Patients with arrhythmic events (N = 25)	Patients without arrhythmic events (N = 12)	OR (95% CI)	*P* value
Male gender [N (%)]	21 (84)	6 (50)	10.44 (0.85–127.48)	.07
Age (years)	30 ± 19	23 ± 18	1.05 (0.99–1.12)	.13
Heart rate (bpm)	69 ± 393	76 ± 473	1.00 (1.00–1.01)	.38
PR interval (ms)	138 ± 19	134 ± 18	0.99 (0.95–1.04)	.84
QRS interval (ms)	86 ± 7	85 ± 10	0.93 (0.82–1.07)	.31
QT interval (ms)	286 ± 36	271 ± 40	1.00 (0.97–1.03)	.75
QTc (ms)	308 ± 29	306 ± 33	0.98 (0.94–1.02)	.33
Early repolarization [N (%)]	22 (88)	2 (17)	46.53 (4.52–478.79)	.001

CI = confidence interval; OR = odds ratio; QTc = corrected QT interval; SQTS = short QT syndrome.
Models were adjusted for gender and age.

Table 3 ECG parameters for study cohorts with short QT interval

	Patients with SQTS	Subjects with short QTc	OR (95% CI)	*P* value
QT_{peak} (ms)	211 ± 37	222 ± 19	0.99 (0.98–1.01)	.37
Corrected QT_{peak}	226 ± 32	234 ± 24	0.99 (0.98–1.01)	.56
T_{peak} to T_{end} (ms)	81 ± 21	67 ± 13	1.08 (1.03–1.13)	<.001
Corrected T_{peak} to T_{end}	89 ± 28	72 ± 17	1.05 (1.02–1.09)	.002
QT_{peak}/QT ratio (%)	27 ± 6	22 ± 4	0.83 (0.73–0.94)	.004

Models were adjusted for gender and age.
CI = confidence interval; OR = odds ratio; QTc = corrected QT interval; SQTS = short QT syndrome.

provides evidence that increased transmural dispersion of repolarization under short QT interval conditions results in ventricular tachyarrhythmia.[38] A tall peaked T wave is one of the characteristic ECG abnormalities in SQTS,[1] but the amplitude of the T wave is not different between patients with SQTS and subjects with short QT interval and no arrhythmic events, suggesting that a tall T wave is associated with a short QT interval but is not associated with arrhythmogenicity.[26] In SQTS, characteristic ECG abnormities are also found in the early repolarization phase. In patients with SQTS, the ECG shows a very short J-point to T-wave peak interval and no flat ST segment.[26] In our study, early repolarization was frequently found in SQTS and was associated with arrhythmic events. Whether the inferolateral J-point elevation reflects late depolarization or early repolarization is controversial, but this pattern has been considered repolarization because of slower inscription, spontaneous changes occurring concurrently with ST segment but not with QRS complexes, and absence of late potentials on signal-averaged ECG.[9,40] Taken together, the finding suggest that abnormalities in the early phase of repolarization create the arrhythmogenic substrate in SQTS.

Sex hormone and gender difference have an important role in the arrhythmia syndromes.[41–43] It is well known that the QT interval is affected by sex hormones, and the QT interval is longer in women than men.[44] Female gender is a risk factor for development of ventricular tachyarrhythmias in both congenital and acquired long QT syndrome.[41,42] On the other hand, Brugada syndrome is more prevalent in men than in women, and the male hormone testosterone is reported to contribute to male predominance in Brugada syndrome.[43] In this study, male gender was associated with arrhythmic events in SQTS and short QT interval was frequently found in men, suggesting a role of sex hormones in SQTS opposite to that in long QT syndrome. Recent evidence that the QT interval can be shortened by anabolic androgenic steroids and testosterone further supports this hypothesis.[45,46]

SQTS is a genetically heterogeneous disease with five responsible genes encoding ion channels: *KCNQ1*, *KCNH2*, *KCNJ2*, *CACNA2D1*, and *CACNB2b*.[3,4] An increase in outward current by gain-of-function mutations in potassium channels or a decrease in inward current by loss of function mutations in calcium channels may be responsible for SQTS.[3,4] Early repolarization was found in patients with mutations in *KCNQ1* and *KCNH2* and in those without mutations in the known genes, suggesting a heterogeneous genetic background for the association between short QT interval and early repolarization. To date, mutations in calcium channel genes (*CACNA2D1* and *CACNB2b*) have been identified in three probands with Brugada syndrome associated with a short QT interval, but early repolarization is not present in the inferolateral leads in any of them.[4] A recent study has identified a mutation in *KCNJ8*, an initial responsible gene for idiopathic ventricular fibrillation associated with early repolarization.[47] Although there are some similarities in phenotype between SQTS and idiopathic ventricular fibrillation with early repolarization, a common genetic background has not been identified.

Conclusion

Our study showed a high prevalence of early repolarization in patients with SQTS and an association of early repolarization with arrhythmic events. Early repolarization may be a useful marker for risk stratification of cardiac arrest in SQTS, although further investigation with longitudinal follow-up is required to evaluate our results.

References

1. Gussak I, Brugada P, Brugada J, et al. Idiopathic short QT interval: a new clinical syndrome? Cardiology 2000;94:99–102.
2. Gaita F, Giustetto C, Bianchi F, et al. Short QT syndrome: a familial cause of sudden death. Circulation 2003;108:965–970.
3. Lehnart SE, Ackerman MJ, Benson DW Jr, et al. Inherited arrhythmias: a National Heart, Lung, and Blood Institute and Office of Rare Diseases workshop consensus report about the diagnosis, phenotyping, molecular mechanisms, and therapeutic approaches for primary cardiomyopathies of gene mutations affecting ion channel function. Circulation 2007;116:2325–2345.
4. Antzelevitch C, Pollevick GD, Cordeiro JM, et al. Loss-of-function mutations in the cardiac calcium channel underlie a new clinical entity characterized by ST-segment elevation, short QT intervals, and sudden cardiac death. Circulation 2007;115:442–449.
5. Brugada R, Hong K, Dumaine R, et al. Sudden death associated with short-QT syndrome linked to mutations in HERG. Circulation 2004;109:30–35.
6. Bellocq C, van Ginneken AC, Bezzina CR, et al. Mutation in the KCNQ1 gene leading to the short QT-interval syndrome. Circulation 2004;109:2394–2397.
7. Priori SG, Pandit SV, Rivolta I, et al. A novel form of short QT syndrome (SQT3) is caused by a mutation in the KCNJ2 gene. Circ Res 2005;96:800–807.
8. Klatsky AL, Oehm R, Cooper RA, et al. The early repolarization normal variant electrocardiogram: correlates and consequences. Am J Med 2003;115:171–177.
9. Haissaguerre M, Derval N, Sacher F, et al. Sudden cardiac arrest associated with early repolarization. N Engl J Med 2008;358:2016–2023.
10. Nam GB, Kim YH, Antzelevitch C. Augmentation of J waves and electrical storms in patients with early repolarization. N Engl J Med 2008;358:2078–2079.
11. Rosso R, Kogan E, Belhassen B, et al. J-point elevation in survivors of primary ventricular fibrillation and matched control subjects: incidence and clinical significance. J Am Coll Cardiol 2008;52:1231–1238.
12. Viskin S. Idiopathic ventricular fibrillation "Le Syndrome d'Haissaguerre" and the fear of J waves. J Am Coll Cardiol 2009;53:620–622.

13. Viskin S. The QT interval: too long, too short or just right. Heart Rhythm 2009;6:711–715.
14. Extramiana F, Maury P, Maison-Blanche P, et al. Electrocardiographic biomarkers of ventricular repolarisation in a single family of short QT syndrome and the role of the Bazett correction formula. Am J Cardiol 2008;101:855–860.
15. Watanabe H, Kaiser DW, Makino S, et al. ACE I/D polymorphism associated with abnormal atrial and atrioventricular conduction in lone atrial fibrillation and structural heart disease: implications for electrical remodeling. Heart Rhythm 2009;6:1327–1332.
16. Anttonen O, Vaananen H, Junttila J, et al. Electrocardiographic transmural dispersion of repolarization in patients with inherited short QT syndrome. Ann Noninvas Electrocardiol 2008;13:295–300.
17. Giustetto C, Di Monte F, Wolpert C, et al. Short QT syndrome: clinical findings and diagnostic-therapeutic implications. Eur Heart J 2006;27:2440–2447.
18. Hong K, Bjerregaard P, Gussak I, et al. Short QT syndrome and atrial fibrillation caused by mutation in KCNH2. J Cardiovasc Electrophysiol 2005;16:394–396.
19. Kirilmaz A, Ulusoy RE, Kardesoglu E, et al. Short QT interval syndrome: a case report. J Electrocardiol 2005;38:371–374.
20. Lu LX, Zhou W, Zhang X, et al. Short QT syndrome: a case report and review of literature. Resuscitation 2006;71:115–121.
21. Mizobuchi M, Enjoji Y, Yamamoto R, et al. Nifekalant and disopyramide in a patient with short QT syndrome: evaluation of pharmacological effects and electrophysiological properties. Pacing Clin Electrophysiol 2008;31:1229–1232.
22. Schimpf R, Wolpert C, Bianchi F, et al. Congenital short QT syndrome and implantable cardioverter defibrillator treatment: inherent risk for inappropriate shock delivery. J Cardiovasc Electrophysiol 2003;14:1273–1277.
23. Viskin S, Zeltser D, Ish-Shalom M, et al. Is idiopathic ventricular fibrillation a short QT syndrome? Comparison of QT intervals of patients with idiopathic ventricular fibrillation and healthy controls. Heart Rhythm 2004;1:587–591.
24. Redpath CJ, Green MS, Birnie DH, et al. Rapid genetic testing facilitating the diagnosis of short QT syndrome. Can J Cardiol 2009;25:e133–e135.
25. Villafane J, Young ML, Maury P, et al. Short QT syndrome in a pediatric patient. Pediatr Cardiol 2009;30:846–850.
26. Anttonen O, Junttila MJ, Maury P, et al. Differences in twelve-lead electrocardiogram between symptomatic and asymptomatic subjects with short QT interval. Heart Rhythm 2009;6:267–271.
27. Peters S, Selbig D. Early repolarization phenomenon in arrhythmogenic right ventricular dysplasia-cardiomyopathy and sudden cardiac arrest due to ventricular fibrillation. Europace 2008;10:1447–1449.
28. Sato A, Furushima H, Hosaka Y, et al. Frequency and characteristics of J-wave. Jpn J Electrocardiol 2009;29(Suppl 3):304.
29. Mehta M, Jain AC, Mehta A. Early repolarization. Clin Cardiol 1999;22:59–65.
30. Hayashi M, Murata M, Satoh M, et al. Sudden nocturnal death in young males from ventricular flutter. Jpn Heart J 1985;26:585–591.
31. Otto CM, Tauxe RV, Cobb LA, et al. Ventricular fibrillation causes sudden death in Southeast Asian immigrants. Ann Intern Med 1984;101:45–47.
32. Garg A, Finneran W, Feld GK. Familial sudden cardiac death associated with a terminal QRS abnormality on surface 12-lead electrocardiogram in the index case. J Cardiovasc Electrophysiol 1998;9:642–647.
33. Letsas KP, Sacher F, Probst V, et al. Prevalence of early repolarization pattern in inferolateral leads in patients with Brugada syndrome. Heart Rhythm 2008; 5:1685–1689.
34. Kamakura S, Ohe T, Nakazawa K, et al. Long-term prognosis of probands with Brugada-pattern ST elevation in V1-V3 leads. Circ Arrhythmia Electrophysiol 2009;2:495–503.
35. Viskin S, Lesh MD, Eldar M, et al. Mode of onset of malignant ventricular arrhythmias in idiopathic ventricular fibrillation. J Cardiovasc Electrophysiol 1997;8:1115–1120.
36. Nam GB, Ko KH, Kim J, et al. Mode of onset of ventricular fibrillation in patients with early repolarization pattern vs. Brugada syndrome. Eur Heart J 2010;31:330–339.
37. Haissaguerre M, Sacher F, Nogami A, et al. Characteristics of recurrent ventricular fibrillation associated with inferolateral early repolarization role of drug therapy. J Am Coll Cardiol 2009;53:612–619.
38. Extramiana F, Antzelevitch C. Amplified transmural dispersion of repolarization as the basis for arrhythmogenesis in a canine ventricular-wedge model of short-QT syndrome. Circulation 2004;110:3661–3666.
39. Shimizu W, Antzelevitch C. Sodium channel block with mexiletine is effective in reducing dispersion of repolarization and preventing torsade de pointes in LQT2 and LQT3 models of the long QT syndrome. Circulation 1997;96:2038–2047.
40. Spach MS, Barr RC, Benson W, et al. Body surface low-level potentials during ventricular repolarization with analysis of the ST segment: variability in normal subjects. Circulation 1979;59:822–836.
41. Hashiba K. Hereditary QT prolongation syndrome in Japan: genetic analysis and pathological findings of the conducting system. Jpn Circ J 1978;42:1133–1150.
42. Makkar RR, Fromm BS, Steinman RT, et al. Female gender as a risk factor for torsades de pointes associated with cardiovascular drugs. JAMA 1993;270: 2590–2597.
43. Shimizu W, Matsuo K, Kokubo Y, et al. Sex hormone and gender difference. Role of testosterone on male predominance in Brugada syndrome. J Cardiovasc Electrophysiol 2007;18:415–421.
44. Furukawa T, Kurokawa J. Regulation of cardiac ion channels via non-genomic action of sex steroid hormones: implication for the gender difference in cardiac arrhythmias. Pharmacol Ther 2007;115:106–115.
45. Bigi MA, Aslani A. Short QT interval: a novel predictor of androgen abuse in strength trained athletes. Ann Noninvas Electrocardiol 2009;14:35–39.
46. Charbit B, Christin-Maitre S, Demolis JL, et al. Effects of testosterone on ventricular repolarization in hypogonadic men. Am J Cardiol 2009;103:887–890.
47. Haissaguerre M, Chatel S, Sacher F, et al. Ventricular fibrillation with prominent early repolarization associated with a rare variant of KCNJ8/KATP channel. J Cardiovasc Electrophysiol 2009;20:93–98.

J Membrane Biol (2010) 235:73–87
DOI 10.1007/s00232-010-9257-2

Characterization of the Rapidly Activating Delayed Rectifier Potassium Current, I_{Kr}, in HL-1 Mouse Atrial Myocytes

Futoshi Toyoda · Wei-Guang Ding · Dimitar P. Zankov · Mariko Omatsu-Kanbe · Takahiro Isono · Minoru Horie · Hiroshi Matsuura

Received: 29 November 2009 / Accepted: 29 April 2010 / Published online: 19 May 2010

Abstract HL-1 is the adult murine cardiac cell line that can be passaged repeatedly in vitro without losing differentiated phenotype. The present study was designed to characterize the rapidly activating delayed rectifier potassium current, I_{Kr}, endogenously expressed in HL-1 cells using the whole-cell patch-clamp technique. In the presence of nisoldipine, depolarizing voltage steps applied from a holding potential of −50 mV evoked the time-dependent outward current, followed by slowly decaying outward tail current upon return to the holding potential. The amplitude of the current increased with depolarizations up to 0 mV but then progressively decreased with further depolarizations. The time-dependent outward current as well as the tail current were highly sensitive to block by E-4031 and dofetilide (IC_{50} of 21.1 and 15.1 nM, respectively) and almost totally abolished by micromolar concentrations of each drug, suggesting that most of the outward current in HL-1 cells was attributable to I_{Kr}. The magnitude of I_{Kr} available from HL-1 cells (18.1 ± 1.5 pA pF^{-1}) was sufficient for reliable measurements of various gating parameters. RT-PCR and Western blot analysis revealed the expression of alternatively spliced forms of mouse *ether-a-go-go*-related genes (mERG1), the full-length mERG1a and the N-terminally truncated mERG1b isoforms. Knockdown of mERG1 transcripts with small interfering RNA (siRNA) dramatically reduced I_{Kr} amplitude, confirming the molecular link of mERG1 and I_{Kr} in HL-1 cells. These findings demonstrate that HL-1 cells possess I_{Kr} with properties comparable to those in native cardiac I_{Kr} and provide an experimental model suitable for studies of I_{Kr} channels.

Keywords Cardiac cell line · Potassium current · Potassium channel · Patch-clamp · HL-1 cell · siRNA

F. Toyoda (✉) · W.-G. Ding · D. P. Zankov · M. Omatsu-Kanbe · H. Matsuura
Department of Physiology, Shiga University of Medical Science, Otsu, Shiga 520-2192, Japan
e-mail: toyoda@belle.shiga-med.ac.jp

D. P. Zankov · M. Horie
Department of Cardiovascular and Respiratory Medicine, Shiga University of Medical Science, Otsu, Shiga 520-2192, Japan

T. Isono
Central Research Laboratory, Shiga University of Medical Science, Otsu, Shiga 520-2192, Japan

Introduction

Cardiac delayed rectifier potassium current (I_K) is responsible for action potential repolarization and pacemaker activity and consists of multiple components with distinct time and voltage dependence and pharmacological properties. I_{Kr} is the rapidly activating, inwardly rectifying component of I_K, which can be isolated as a fraction specifically blocked by the class III antiarrhythmic methanesulfonanilide agents such as E-4031 and dofetilide (Sanguinetti and Jurkiewicz 1990). It is now well known that I_{Kr} is conducted by ERG1 (*ether-a-go-go*-related gene) potassium channels (Sanguinetti et al. 1995; Trudeau et al. 1995). Mutations in the human ERG1 (HERG) channel gene underlie the inherited long QT syndrome, a disorder of cardiac repolarization that predisposes affected individuals to life-threatening arrhythmias (Curran et al. 1995). In addition, I_{Kr} is sensitive to block by a diverse range of therapeutic agents (e.g., antihistamines, gastrointestinal prokinetic agents, psychoactive substances), and these adverse drug effects can induce acquired long QT syndrome (Roden et al. 1996).

Taking advantage of molecular biological technology, functional analysis of reconstituted HERG channels in a heterologous expression system has provided information on the gating mechanisms, modulation and drug block of I_{Kr} channels. Nevertheless, current recordings from native channels are still important because several differences between native I_{Kr} and reconstituted HERG current have been revealed (Sanguinetti et al. 1995; Weerapura et al. 2002), possibly due to inadequate composition of channel proteins or lack of cardiac-specific environments in the heterologous expression system. AT-1 cells, a cardiac cell line derived from atrial tumor of adult transgenic mice expressing the simian virus 40 (SV40) large T-antigen targeted to atrial cardiomyocytes via the atrial natriuretic factor (ANF) promoter (Field 1988), have been often employed as a suitable source of native I_{Kr} channels (Liu et al. 1994; Yang and Roden 1996; Yang et al. 1994, 1995, 1997). Membrane current recorded from these cells displays phenotypical characteristics of cardiac I_{Kr} with minimal contamination of other time-dependent outward currents. Maintenance of AT-1 cells, however, is complicated and labored because it is impossible to passage these cells serially in vitro. They are maintained by serial propagation as a subcutaneous tumor in syngeneic mice and have to be used as primary cells (Delcarpio et al. 1991).

The HL-1 cell line was derived from subsequent development of AT-1 cells (Claycomb et al. 1998). Different from any other cardiac cell lines currently available, HL-1 cells can be repeatedly passaged in culture while maintaining a differentiated cardiac phenotype. They express many cardiac-specific proteins such as α-myosin heavy chain, ANF, α-cardiac actin and connexin 43 (Claycomb et al. 1998). Furthermore, several functional receptors, such as α_1-adrenergic and δ-opioid receptors, and intracellular signaling proteins required for phosphatidylinositol hydrolysis and the cyclic AMP synthesis pathway have been demonstrated in HL-1 cells (McWhinney et al. 2000; Neilan et al. 2000; Sartiani et al. 2002). Recent patch-clamp studies have revealed the existence of several cardiac membrane currents, including I_{Kr} as well as the hyperpolarization-activated nonselective cation current (I_f) and the L- and T-type Ca^{2+} currents ($I_{Ca,L}$ and $I_{Ca,T}$) (Claycomb et al. 1998; Sartiani et al. 2002; Xia et al. 2004; Zankov et al. 2009). Thus, HL-1 cells may be used as a model of cardiac cells for studying many features of ion channels in a cardiac-specific environment (White et al. 2004).

The present study characterizes I_{Kr} channels endogenously expressed in HL-1 cells. Whole-cell patch-clamp experiments demonstrate that I_{Kr}, defined as the E-4031-sensitive current, can be elicited in almost all cells with current magnitude of 0.1–1.5 nA suitable for high-quality recording, which allows us to analyze biophysical and pharmacological features extensively and reliably. In addition, alternatively spliced forms of mouse ERG1 (mERG1) are identified in HL-1 cells, and our RNA interference (RNAi) experiments suggest that these ERG1 isoforms indeed underlie I_{Kr}. Data obtained here will be helpful for future applications of HL-1 cells as a unique model to study cardiac I_{Kr} channels.

Methods

Culture of HL-1 Cells

The HL-1 cell culture (passage 36) was a kind gift from Dr. Claycomb (Louisiana State University Health Science Center, New Orleans, LA) who first established the cell line. Care of the HL-1 cells was described previously (Claycomb et al. 1998). Claycomb medium (JRH Bioscience, Lenexa, KS; catalog 51800), a commercially available medium specifically designed for the growth of HL-1 cells, was purchased. Before use, the Claycomb medium was supplemented with 10% fetal bovine serum (JRH Bioscience), 2 mM L-glutamine (Invitrogen, Carlsbad, CA), 0.1 mM norepinephrine (Sigma, St. Louis, MO) and penicillin–streptomycin (Nakalai Tesque, Kyoto, Japan). The supplemented Claycomb medium was prepared every 2 weeks and kept in the dark by covering the medium bottle with aluminum foil because it is highly light-sensitive. Cells were plated on T25 flasks (Techno Plastic Products, Trasadingen, Switzerland; 90025) precoated overnight with 0.00125% fibronectin (Sigma, F1141) in 0.02% gelatin (Difco, Detroit, MI; 0143-17-9) and maintained in supplemented Claycomb medium at 37°C in humidified 5% CO_2 and 95% air. The culture medium was changed daily. After full confluence, cells were dissociated by 0.05% trypsin/EDTA (Invitrogen). Isolated cells were then suspended in Claycomb medium supplemented with 5% fetal bovine serum and antibiotics, and the cell suspension was used for the patch-clamp experiments or split into new flasks for subsequent culturing.

Reverse Transcription-Polymerase Chain Reaction Amplification

HL-1 cells culture (passage 40) and atrial tissue dissected from adult mice were used for mRNA purification. Total RNA from each sample was extracted by the acid guanidium thiocyanate chlorofrom method (Chomczynski and Sacchi 1987). cDNA was synthesized from 5 μg of total RNA with 20 units of RAV-2 reverse transcriptase (Takara, Otsu, Japan) using random primers. PCR for mouse ERG1 isoforms (mERG1a, mERG1a′ and mERG1b) was

performed using the following primer sets reported previously (Clark et al. 2004) (from 5 to 3): ACA CCT TCC TCG ACA CCA TC (sense; position 621–641, accession AF012870) and GCA TCA GGG TTA AGG CTC TG (antisense; position 1405–1424, accession AF012871) for mERG1a, ACC ACT GGC ATA GGA CCA AG (sense; position 839–858, accession AF012870) and the same antisense as for mERG1a for mERG1a′, ATG GCG ATT CCA GCC GGG AA (sense; position 3952–3971, accession AF012871) and GAT GCC ATT GGT GTA GGA CC (antisense; position 8239–8258, accession AF012871) for mERG1b. The reaction included 0.4 µl of cDNA, 2.5 units of KOD dash polymerase (Toyobo, Osaka, Japan), 1 mM KCl, 6 mM $(NH_4)_2SO_4$, 0.1% Triton X-100, 10 µg ml^{-1} BSA, 0.2 mM each of deoxynucleotide triphosphate and 4 pmol primers in 20 ml of 120 mM Tris–HCl buffer (pH 8.0). Amplification was conducted in a thermal cycler using 30 cycles consisting of denaturation at 98°C for 2 s, annealing at 55°C for 2 s and elongation at 72°C for 60 s. PCR products were identified in an ethidium bromide-stained 1.5% agarose gel by electrophoresis.

Western Blotting

HL-1 cells (passages 45–47) were washed with cold phosphate-buffered saline and resuspended in lysis buffer (50 mM Tris–HCl, 5 mM EDTA, 150 mM NaCl, 1% Triton X-100, pH 7.4) supplemented with a mix of protease inhibitors (Complete Mini; Roche, Mannheim, Germany). Cell lysate was centrifuged at 15,000 rpm for 5 min. Total protein was measured using the DC protein assay (Bio-Rad, Richmond, CA). For Western blot assay, 100 µg of total proteins were dissolved in 2 × SDS sample buffer (4% sodium dodecyl sulfate, 125 mM Tris–HCl, 12% 2-mercaptoethanol, 20% glycerol, 0.005% bromophenol blue, pH 6.8) and then sonicated and boiled for 5 min. Samples were resolved on 7.5% SuperSep gel (Wako, Osaka, Japan) and electrotransferred onto a polyvinylidene difluoride (PVDF) membrane (Bio-Rad). The membrane was blocked in Tris-buffered saline (TBS; 10 mM Tris–HCl, 100 mM NaCl, pH 7.5) containing 0.1% Tween-20 and 10% nonfat dry milk for 1.5 h at room temperature and then incubated overnight at 4°C with a rabbit polyclonal anti-ERG1 antibody (Chemicon, Temecula, CA; AB5222) directed against the C terminus (amino acid residues 1121–1137, accession O08962) of rat ERG1, at a dilution 1:200. After washing with TBS-Tween 0.1%, the membrane was incubated with a horseradish peroxidase-conjugated secondary anitibody (Jackson ImmunoResearch, West Grove, PA; 1:5,000) for 1 h at room temperature. Signals were detected using an enhanced chemiluminescence system.

RNAi

Two Stealth small interfering RNA (siRNA) duplex oligonucleotides directed against all transcripts of the mERG1 gene and RNAi-negative control duplex oligonucleotide (ncRNA) were provided by Invitrogen. The siRNA sequences were as follows: siRNA-1, 5′-AGG CUG ACA UCU GCC UAC ACC UGA A-3′; siRNA-2, 5′-UGU CAU UCC GCA GGC GUA CAG ACA A-3′. HL-1 cell culture of nearly confluent (passages 42–45) was transfected with siRNA against mERG1 or nonspecific RNA (ncRNA, 50 pmol), together with a reporter plasmid DNA (pEGFP vector, 0.5 µg) using Lipofectamine 2000 reagent (Invitrogen) according to the manufacture's instructions. Only GFP-positive cells 2 days after transfection were employed for electrophysiological experiments.

Patch-Clamp Recordings

Current recordings from HL-1 cells (passages 38–52) were performed using the whole-cell configuration of the patch-clamp technique (Hamill et al. 1981) with an EPC-8 patch-clamp amplifier (Heka, Lambrecht, Germany). Cells were dissociated from culture dishes by 0.05% trypsin/EDTA, suspended in Claycomb medium and stored at 4°C for a few hours before use. A small aliquot of cell suspension was transferred into a small (0.5 ml) recording chamber placed on the stage of an inverted microscope (TMD-300; Nikon, Tokyo, Japan). After settling to the glass bottom of the chamber (5–10 min), the cells were continuously superfused with normal Tyrode solution (containing appropriate drugs) kept at 25 ± 1°C or 35 ± 1°C, as indicated. Patch-clamp pipettes were prepared from glass capillary tube (Narishige, Tokyo, Japan) on a horizontal pipette puller (P-97; Sutter Instrument, Novato, CA), and the tips were then fire-polished by a microforge (MF-83, Narishige). Pipette resistance was 2–4 MΩ when filled with internal solution. Currents and voltages were digitized and voltage commands were generated through an ITC-16 AD/DA interface (InstruTECH, Long Island, NY) controlled by Pulse/Pulsefit software (version 8.54, Heka).

Data Analysis

Membrane capacitance (C_m) was calculated by fitting a single exponential function to the decay phase of the transient capacitive current in response to ±5-mV voltage steps (20 ms) from a holding potential of −50 mV. The current amplitude was divided by C_m to obtain the current density (pA pF^{-1}). Linear regression analysis was used for correlations. The voltage dependence of current activation and inactivation was determined by fitting the normalized

tail current (I_{tail}) vs. test potential (V) to a Boltzmann function expressed by $I_{tail} = 1/(1 + \exp[(V_{1/2} - V)/k])$ and $I_{tail} = 1/(1 + \exp[(V - V_{1/2})/k])$, respectively, where $V_{1/2}$ is the voltage at which the current is half-activated and k is the slope factor. The time constant for activation (τ_{act}) was determined from a single-exponential fit to the envelop of tail currents obtained after depolarizing pulses for varying durations, and time constants for deactivation (τ_{fast} and τ_{slow}) were obtained by fitting a two-exponential function to the time course of deactivating tail currents. Dose responses for drug block of currents were analyzed by fitting the relative amplitudes of tail currents (y/y_{max}) vs. the drug concentration ([D]) to a Hill function: $y/y_{max} = 1/\{1 + (IC_{50}/[D])^n\}$, where IC_{50} is the half-inhibitory concentration and n is the Hill coefficient. Data were expressed as mean ± SEM. Statistical analysis was performed by means of ANOVA and a post hoc Tukey test.

Solutions and Drugs

Normal Tyrode solution contained (mM) 140 NaCl, 0.33 NaH_2PO_4, 5.4 KCl, 1.8 $CaCl_2$, 0.5 $MgCl_2$, 5.5 glucose and 5 HEPES, pH adjusted to 7.4 with NaOH. The external solution for current recording was made by adding 0.4 μM nisoldipine (as 1 mM stock solution in ethanol) to normal Tyrode solution to eliminate $I_{Ca,L}$. In some experiments, the concentration of KCl was modified to 2 or 10 mM. The internal pipette solution contained (mM) 70 potassium aspartate, 50 KCl, 10 KH_2PO_4, 1 $MgCl_2$, 3 Na_2–ATP, 0.1 Li_2–GTP, 5 EGTA and 5 HEPES, pH adjusted to 7.2 with KOH. Liquid junction potential between the test solution and the pipette solution was measured at around −10 mV and corrected. In order to rule out possible contamination of $I_{Ca,L}$ in our data, all experiments were conducted in the presence of 0.4 μM nisoldipine (a generous gift from Bayer AG, Wuppertal-Elberfeld, Germany), which is specific blocker of $I_{Ca,L}$. E-4031 (Wako), dissolved in distilled water (1 mM) and dofetilide (a generous gift from Pfizer, Sandwich, UK), dissolved in acidified water (pH 4.0, 1 mM), were diluted down to the final concentration in the test solution.

Results

E-4031-Sensitive Current in HL-1 Cells

I_{Kr} was originally identified as a methanesulfonanilide-sensitive component of I_K in guinea pig cardiomyocytes (Sanguinetti and Jurkiewicz 1990). We recorded whole-cell membrane currents from single HL-1 cells before and after application of E-4031 and then analyzed a drug-sensitive current (Fig. 1). Possible participation of other voltage-dependent currents in our data was minimized; i.e., 0.4 μM nisoldipine was included in the bath solution to block $I_{Ca,L}$ (Xia et al. 2004) and membrane potential was held at −50 mV to inactivate $I_{Ca,T}$ (Xia et al. 2004) and avoid I_f activation (Sartiani et al. 2002). Figure 1a shows representative membrane currents in response to 1-s depolarizing (upper panel) and hyperpolarizing (lower panel) pulses to various test potentials, ranging between −80 and +40 mV in 10-mV steps from a holding potential of −50 mV. As shown in the upper panel of Fig. 1a, depolarizing steps activated time-dependent outward currents with amplitudes that increased with depolarization up to 0 mV and then progressively decreased as the potential became more positive (filled circles, Fig. 1d). After return of the membrane to the holding potential, slowly deactivating tail currents were elicited. In contrast, as shown in the lower panel, hyperpolarizing steps induced small-amplitude inward currents with a slight time dependence, which was possibly due to activation of I_f channels, and following depolarizing steps to the holding potential elicited transient inward currents, which may be attributed to activation of $I_{Ca,T}$. When E-4031 (5 μM) was applied to the bath solution, the time-dependent outward current during depolarizing steps as well as the tail current were almost completely abolished, whereas the inward current during the hyperpolarizing pulse was not significantly influenced (Fig. 1b). The currents after exposure to the drug were nearly time-independent and exhibited small conductance with slight outward rectification (open circles in Fig. 1d). E-4031-sensitive currents obtained by digital subtraction of current traces in the presence of drug from those before application of the drug are illustrated in Fig. 1c. The drug-free and the E-4031-sensitive currents showed very similar current–voltage relationships, and both currents have the characteristics of inward rectification at more positive potential than 0 mV, indicating that I_{Kr} is the dominant outward current in HL-1 cells.

The voltage dependence for I_{Kr} activation was determined by measuring the tail amplitude of E-4031-sensitive current. Figure 2a shows the initial part of tail currents elicited upon return of the membrane potential to −50 mV from the 1-s depolarizing steps to test potentials ranging from −40 to +40 mV. The tail current obviously activated at −30 mV and increased in amplitude for the steps up to +10 mV. In Fig. 2b, the amplitude of the tail currents was normalized to the maximum tail current amplitude and plotted as a function of the membrane potential. The $V_{1/2}$ and k, which were determined by curve fitting the data points to a Boltzmann equation, were −20.4 and 8.0 mV, respectively.

In Fig. 3, kinetic properties were determined by measuring time constants for apparent activation and deactivation of I_{Kr}. An envelope-of-tails test was used to assess

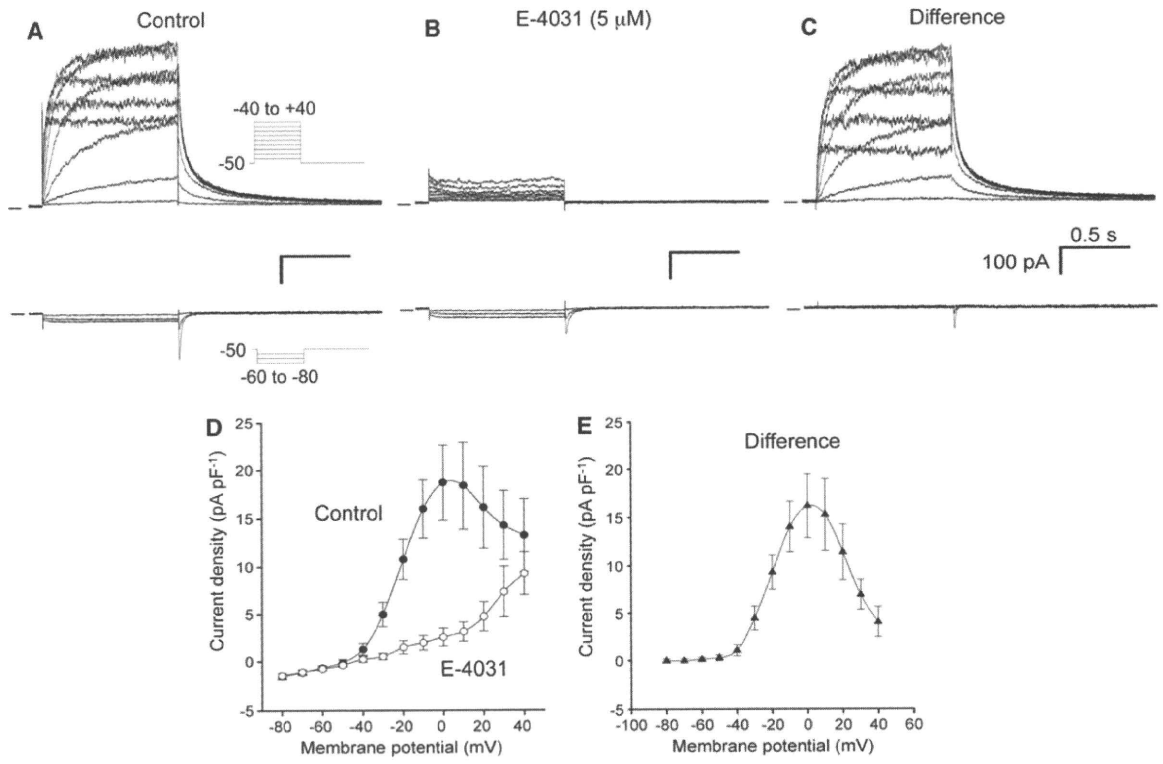

Fig. 1 E-4031-sensitive current recorded from isolated HL-1 cells. **a**, **b** Superimposed whole-cell membrane currents recorded from single HL-1 cell (passage 38) before (**a**) and after (**b**) exposure to 5 μM E-4031. The cell was held at −50 mV and given 1-s depolarizing (between −40 and +40 mV, *upper panel*) and hyperpolarizing (between −80 and −60 mV, *lower panel*) test pulses. The experiment was conducted at 35°C. **c** E-4031-sensitive current obtained from digital subtraction of two traces in **a** and **b**. **d** Average current–voltage relationships recorded before (*filled circles*) and after (*open circles*) exposure to E-4031. Current amplitudes measured just before the end of the 1-s pulses were plotted against the indicated membrane potentials. Values represent mean ± SEM of 10 HL-1 cells (passages 38–41). **e** Current–voltage relationship for E-4031-sensitive currents

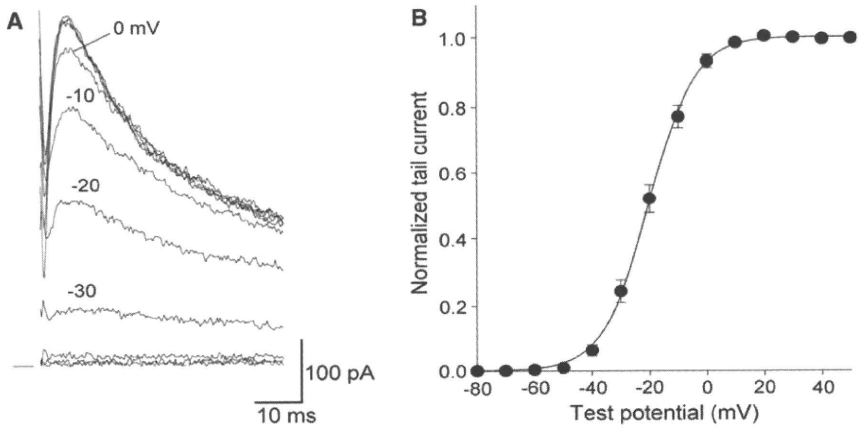

Fig. 2 Voltage-dependent activation of E-4031-sensitive current in HL-1 cells. **a** Representative tails of E-4031-sensitive current recorded from an HL-1 cell (passage 38). Tail currents were elicited on repolarization to −50 mV, following 1-s depolarization to +20 mV. **b** Voltage dependence of E-4031-sensitive current. Tail current amplitudes were normalized to the maximal value at +20 mV, and averaged data were plotted against the indicated test potentials. Values represent mean ± SEM of 10 HL-1 cells (passages 38–41). *Smooth curve* represents fitting of the data to the Boltzmann equation

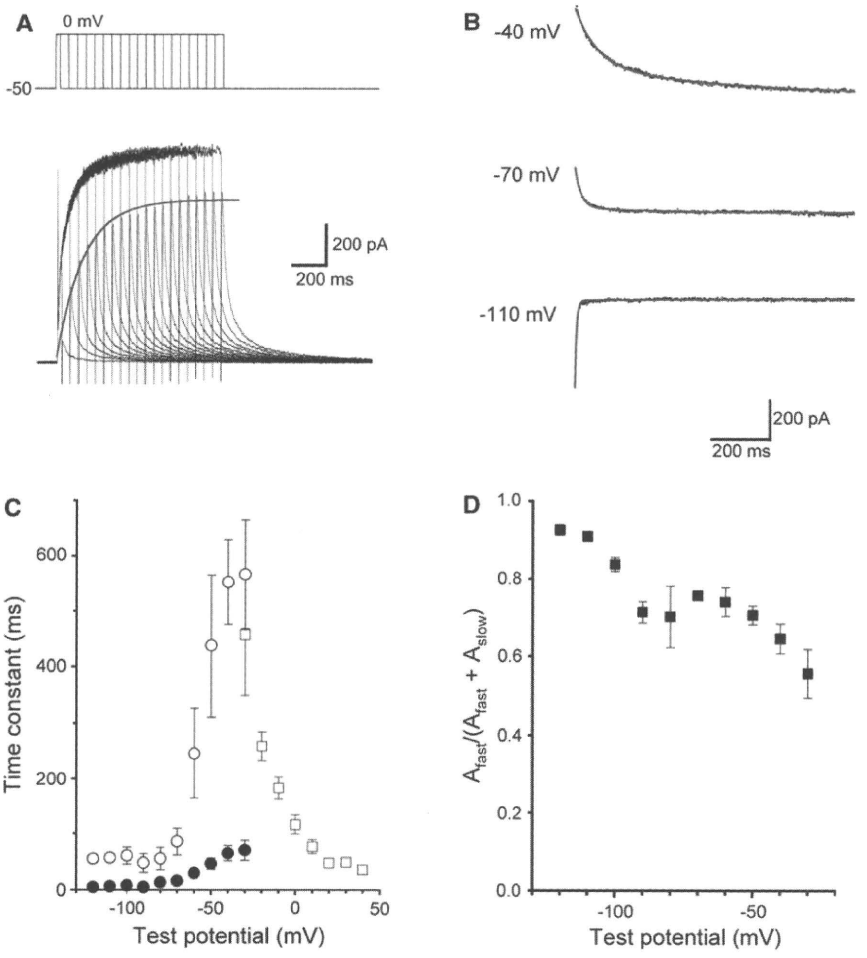

Fig. 3 Activation and deactivation kinetics. **a** Activation time courses assessed with an envelope-of-tails protocol. Original current traces recorded from an HL-1 cell (passage 44) in response to the depolarizing steps to 0 mV of varying duration (25–975 ms in 50-ms increments) from a holding potential of −50 mV. *Solid curve* is a single-exponential fit to the peak tail current elicited upon repolarization to the holding potential. **b** Deactivation time courses of E-4031-sensitive current recorded from an HL-1 cell (passage 39). Decaying phase of tail currents (*dots*) elicited at −40, −70 and −110 mV after depolarizing prepulse to +20 mV of 1-s duration were fit to a sum of two exponential equations (*solid line*). **c** Average voltage dependence of time constants for the apparent activation (*open squares*) and the fast (*open circles*) and slow (*filled circles*) components of deactivation of the E-4031-sensitive current. **d** Voltage dependence of the relative amplitude of the fast component in decaying tail current. Values represent mean ± SEM of four to 10 cells (passages 38–47)

the time course of activation. Figure 3a shows a representative example of current traces in response to depolarizing test pulses to 0 mV of varying duration (25–975 ms in 50-ms increments). The tail current amplitude on return to the holding potential reflects the extent of I_{Kr} activation produced during depolarization to 0 mV, which was well fitted by a single-exponential function, where the τ value was 162.8 ms. The kinetics was steeply voltage-dependent and the activation time constants decreased with incremental changes in the test potentials (τ_{act}, open squares in Fig. 3c). Time constants of deactivation were calculated by fitting the decay of tail currents at various test potentials between −120 and −20 mV following 1-s depolarizing pulses to +20 mV to a double-exponential function, as shown in Fig. 3b. In contrast to activation, the deactivation time course was accelerated at more negative potentials. As summarized in Fig. 3c, both the fast (τ_{fast}, filled circles) and slow (τ_{slow}, open circles) time constants of deactivation were increased as the test potential became more positive. The slow time constants of deactivation at −30 mV were comparable to the time constant of activation at the same potential, and they were plotted as a bell-shaped function of the membrane potential. Figure 3d shows a plot of the relative amplitude of the fast component, $A_{fast}/(A_{fast} + A_{slow})$, of decaying tail current against the membrane potential. The value decreased from approximately 0.9 to 0.5 over the membrane potential from −120 to −20 mV.

I_{Kr} Density in HL-1 Cells

There was a large cell-to-cell variation in HL-1 cell size even in the same culture; C_m measured in patch-clamp experiments ranged between 5.4 and 84.0 pF (mean ± SEM, 29.9 ± 2.3 pF). We tested whether ununiformity of cell size reflects their functional heterogeneity of I_{Kr} channel. The relationship between I_{Kr} density and C_m was investigated in 69 cells (Fig. 4a). The I_{Kr} density ranged between

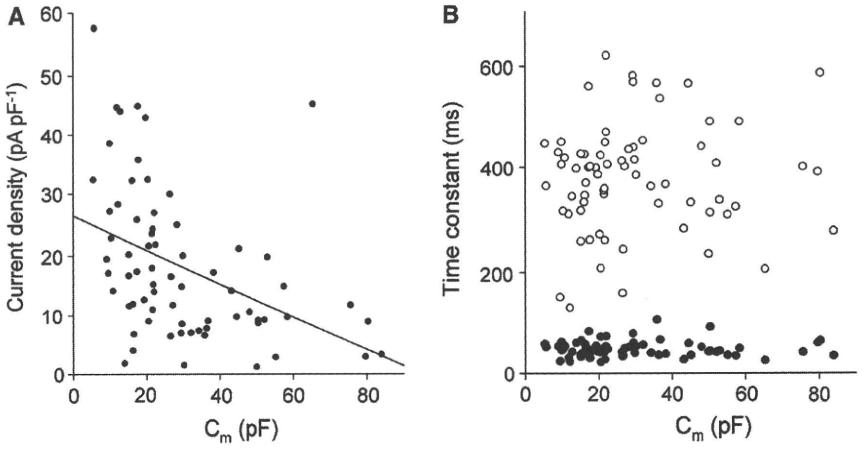

Fig. 4 Relationships between HL-1 cell size and E-4031-sensitive current. Scatter plots of the current density (**a**) and the deactivation time constants (**b**) of the slow (*open circles*) and fast (*filled circles*) components, measured in E-4031-sensitive tail current elicited by a voltage step to −50 mV after 1-s depolarization to +20 mV, against the membrane capacitance of individual cells. Data were obtained from HL-1 cells (passages 38–52)

1.2 and 57.5 pA pF^{-1} (18.1 ± 1.5 pA pF^{-1}, $n = 69$), which was roughly and negatively correlated with cell size ($r = -0.42$, $P < 0.0003$). On the other hand, no obvious correlation between deactivation kinetics of I_{Kr} and cell size was observed (Fig. 4b).

Voltage Dependence of I_{Kr} Inactivation in HL-1 Cells

The shape of the I_{Kr} tail current (initial "hook" or increase in amplitude, followed by slower decay) reflects the presence of a biphasic process during repolarization. The initial increasing phase of the tail current preceding a decay in amplitude has been shown to reflect a recovery from inactivation that occurs much faster than deactivation (Sanguinetti and Jurkiewicz 1990; Shibasaki 1987). In Fig. 5, the rate of recovery from inactivation was estimated. The currents were elicited by voltage pulses to various test potentials between −120 and −10 mV after the 1-s preconditioning pulses to +20 mV. Experiments were conducted at 25°C to allow discrimination of the onset of tail currents from capacitive transients. In Fig. 5a, a set of current traces during test steps is shown. Increment phases of the tail current were well fitted by a single-exponential function with smaller time constants at more negative potentials. For example, the averaged τ value at −120 mV was 0.92 ± 0.04 ms, while it increased to 10.50 ± 0.74 ms at −10 mV (Fig. 5b).

The voltage dependence of current inactivation was examined using a three-pulse protocol (inset in Fig. 6a) (Smith et al. 1996), in which the cell was depolarized to +20 mV for 1 s to activate and inactivate I_{Kr} channels,

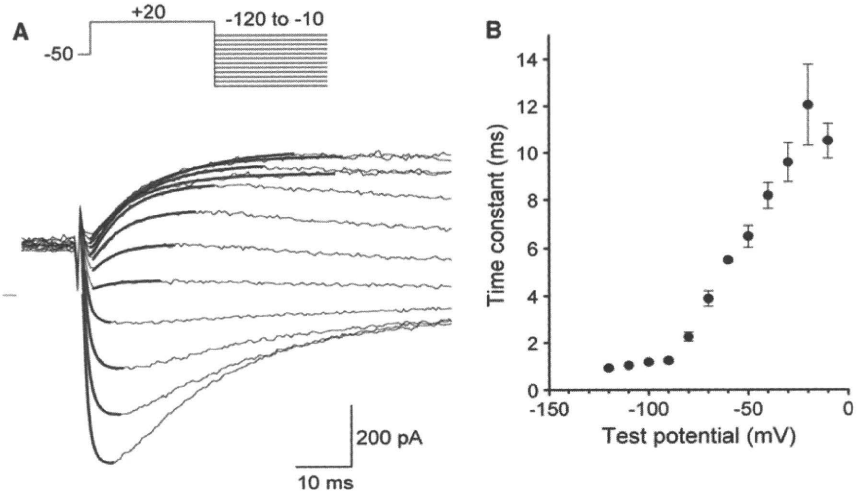

Fig. 5 Kinetic properties of recovery from inactivation. **a** The "hook" tail currents (*thin line*) elicited by voltage steps to various potentials between −120 and −10 mV in 10-mV intervals following the 1-s depolarizing steps to +20 mV (*inset*). Current recording was conducted at 25°C. *Smooth curves* (*thick line*), superimposed to initial increasing phase in amplitude, are obtained by a single-exponential fit. **b** Voltage dependence of the rate of recovery from inactivation. Time constants, measured in (**a**), were plotted against each test potential. Values represent mean ± SEM of four cells (passages 41, 42)

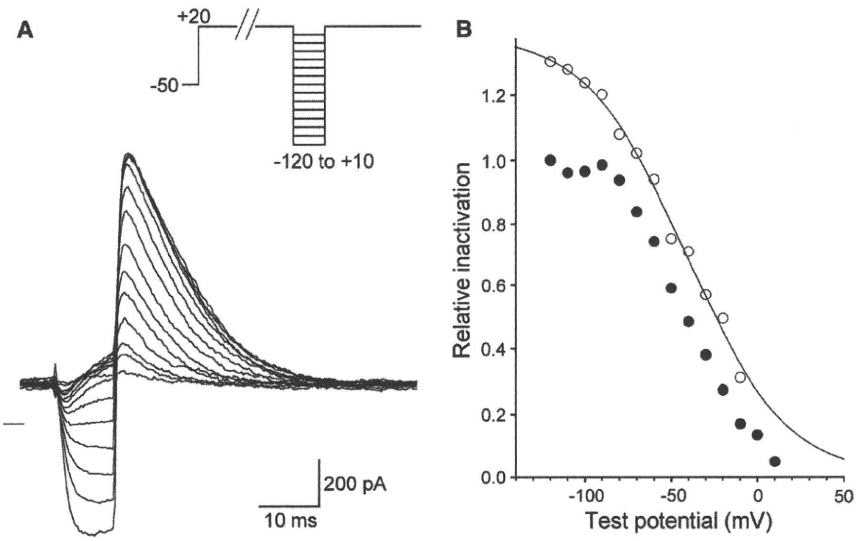

Fig. 6 Voltage dependence of steady-state inactivation. **a** E-4031-sensitive current recorded from an HL-1 cell (passage 41) in response to three-pulse protocol (*inset*). At first, a depolarizing pulse of more than 1 s duration to +20 mV (P1) was applied, where current was activated and inactivated rapidly. Then, a hyperpolarizing test pulse of 10 ms to a varied potential (P2) was used to allow recovery from inactivation, followed by a step to +20 mV (P3). *Dashed line* represents zero current level. Current recording was conducted at 25°C. **b** Current amplitude in response to the P3 pulse (*filled circles*) was normalized to the maximal amplitude at −120 mV and plotted against the test potentials. At negative voltages (≤−60 mV), significant deactivation occurred during 10 ms of the P2 repolarizing step. In addition, at less negative potential (>−70 mV), increasing phase current did not reach the steady-state level during the P2 step. Therefore, the fractional deactivation and incomplete recovery from inactivation during 10 ms were calculated using kinetic parameters (obtained from current traces in Fig. 5), and the data points were corrected to the steady-state inactivation level (*open circles*). Corrected values were well fitted by the Boltzmann equation (*smooth curve*)

then briefly (10 ms) repolarized to various test potentials between −120 and +10 mV to allow for recovery from inactivation without significant deactivation of the channels. After the brief steps, a depolarizing step to +20 mV was applied to evaluate the relative number of opening channels. Figure 6a shows a part of the current traces in response to the pulse protocol (as indicated in the inset). During the brief repolarization, the currents relaxed rapidly to the appropriate level to the corresponding test potentials. Then, depolarizing pulses to +20 mV elicited a large amplitude of outward currents that decayed to the steady-state level within 40 ms due to rapid inactivation. The peak amplitude of the outward currents was measured and plotted against test potentials as filled circles in Fig. 6b. Smith et al. (1996) described that the current amplitude at negative voltages (≤−60 mV) should be corrected because fast deactivation occurred during the brief repolarization. Furthermore, the recovery from inactivation also might not reach the steady-state level at depolarized potential (>−70 mV). Thus, the fractional deactivation and recovery from inactivation during 10-ms repolarizing steps were corrected with respect to the steady-state inactivation level (open circle in Fig. 6b). The half-maximal inactivation voltage calculated by fitting the corrected data to a Boltzmann function was −41.2 mV and the slope factor was 28.9 mV.

K^+ Permeability of I_{Kr} in HL-1 Cells

In Fig. 7, the effects of $[K^+]_o$ on the reversal potential (E_{rev}) of the tail current were investigated. Cells were bathed in Tyrode solution containing 2, 5.4 (normal) and 10 mM KCl; and tail currents were recorded at various test potentials between −120 and 0 mV in 10-mV steps following the 1-s preconditioning pulses to +20 mV (Fig. 7a). The tail current amplitudes were measured and plotted against test potentials in Fig. 7b. At all $[K^+]_o$ conditions, the current–voltage relationships were nearly linear at the potential range between −140 and −80 mV and prominent inward rectification was observed at more positive potential than −70 mV. The conductance at potentials between −140 and −80 mV, measured by fitting lines with a liner regression, was increased with incremental change in $[K^+]_o$ (10.6, 14.1 and 19.7 pS at 2, 5.4 and 10 mM $[K^+]_o$, respectively). E_{rev}, where the polarity of the tail current is reversed, was obtained from a linear regression of the data points between −140 and −70 mV. E_{rev} values at 2, 5.4 and 10 mM $[K^+]_o$ were −115, −91 and −76 mV, respectively, very near the calculated

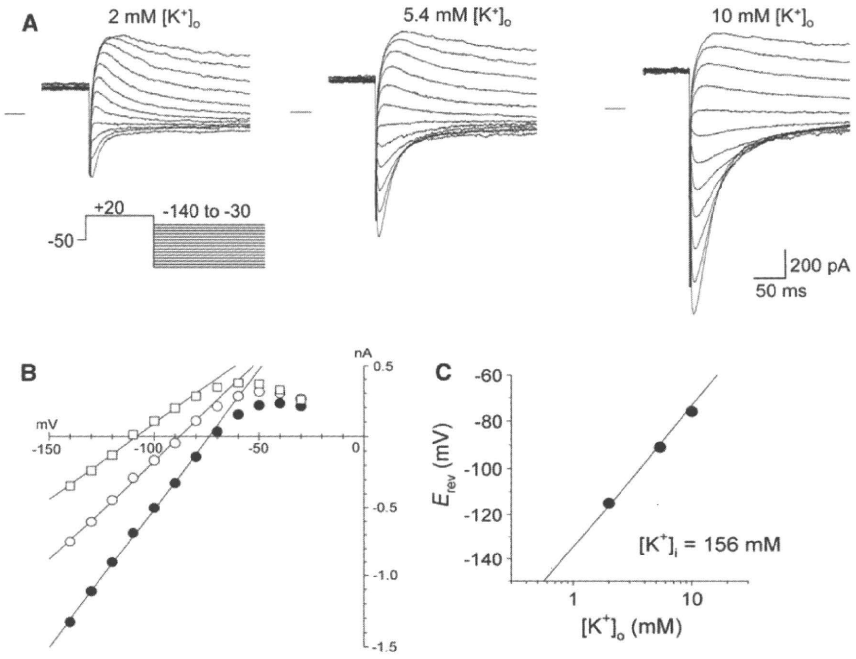

Fig. 7 Effects of extracellular K^+ concentrations on E-4031-sensitive currents. **a** Tail currents recorded at 2 (*left*), 5.4 (*middle*) and 10 mM $[K^+]_o$ conditions (*right*) at 25°C. The cell (passage 39) was initially depolarized to +20 mV from a holding potential of −50 mV, followed by test steps to various potentials between −120 and −30 mV (voltage protocol, *inset*). **b** Tail current amplitude at 2 (*open squares*), 5.4 (*open circles*) and 10 mM $[K^+]_o$ conditions (*filled circles*) shown as a function of test potentials. *Solid lines* on the plot were obtained by a linear regression of data points between −140 and −70 mV: $I_{tail} = g_{max} \cdot (E - E_{rev})$, where g_{max} and E_{rev} were, respectively, 10.6 pS and −115 mV at 2 mM $[K^+]_o$, 14.1 pS and −91 mV at 5.4 mM $[K^+]_o$ and 19.7 pS and −76 mV at 10 mM $[K^+]_o$. **c** Relationships between $[K^+]_o$ and E_{rev}. E_{rev} values in (**b**), plotted against each $[K^+]_o$ concentration, were in good agreement with a predicted E_K (*solid line*) calculated using a Nernst equation, $E_K = RT/F \cdot \ln([K^+]_o/[K^+]_i)$, where $[K^+]_i$ was assumed to be 158 mM

equilibrium potential of K^+ of −116, −89 and −73 mV, respectively (Fig. 7c).

Blocking Effects of E-4031 and Dofetilide on I_{Kr} in HL-1 Cells

In Fig. 8, the blocking effects of methanesulfonanilide drugs E-4031 and dofetilide on I_{Kr} in HL-1 cells were determined. The 1-s depolarizing pulses to +20 mV were repetitively given to the cells every 8 s to activate I_{Kr}, and the blocking effects of the drugs were determined by reduction of tail current elicited at −50 mV. Figure 8a shows the time course of changes in tail current amplitude during application of E-4031 at various concentrations as indicated. In the absence of drugs, the magnitude of the tail current was stable. Exposure to 10 nM E-4031 gradually reduced the tail currents by about 20% at the steady-state level, and the blocking effects increased as the drug concentration became higher. The IC_{50} values for block of tail currents by dofetilide and E-4031 were estimated to be 15.1 and 21.2 nM, respectively; and both drugs inhibited tail current completely at 1 μM (Fig. 8b, c).

Mouse ERG1 Expression Underlies I_{Kr} in HL-1 Cells

In Fig. 9, mERG1 expression in HL-1 cells was investigated with RT-PCR and Western blot assay. It has been reported that there are at least three isoforms of ERG1 at the mRNA level in human and mouse, i.e., the full-length ERG1a and two alternative splicing variants, ERG1a′ and ERG1b, with shorter N termini (Lees-Miller et al. 1997; London et al. 1997). In the present study, therefore, primer pairs directed to each ERG1 isoform were used for PCR amplification. Figure 9a shows an agarose gel of amplified PCR products, where specific bands of the expected size are detected for mERG1a (747 bp), mERG1a′ (755 bp) and mERG1b (1,109 bp) only in the presence of transcriptase. A similar gene expression profile was also detected in adult mouse atrial tissue (Fig. 9b). In order to examine protein expression, we employed an anti-ERG1 antibody that recognizes a common C-terminal epitope in all three mERG1 isoforms. As shown in Fig. 9c, the C-terminal ERG1 antibody identified several bands on a Western blot of HL-1 cells. The two higher bands with molecular mass of 120 and 160 kDa are consistent with maturely

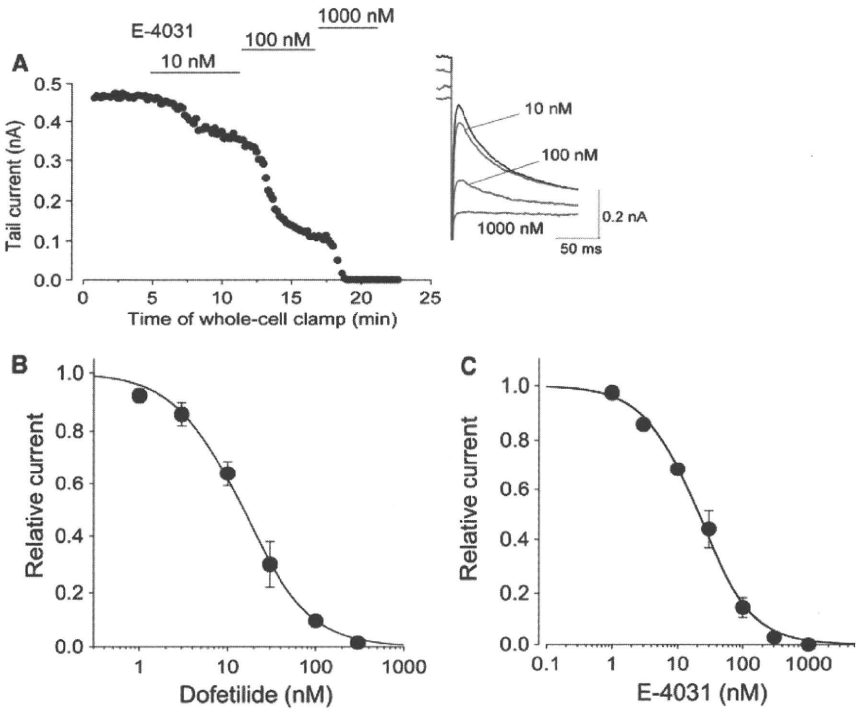

Fig. 8 Inhibitory effects of E-4031 and dofetilide on I_{Kr} in HL-1 cells. **a** Time course of changes in tail current amplitude during exposure to E-4031. Tail currents, as shown in *inset*, were elicited by a voltage step to −50 mV after 1-s depolarization to +20 mV. E-4031 was applied at various concentrations as indicated. **b**, **c** Dose-response relationships of blocking effects of E-4031 (**b**) and dofetilide (**c**). Tail current amplitude was normalized to the maximal amplitude in the absence of drug and plotted against each drug concentration. Data points represent mean ± SEM of five cells (passages 41–52). *Smooth curve* was obtained by fitting the data with a Hill equation, where IC_{50} and Hill coefficient were, respectively, 15.1 nM and 1.2 in (**b**) and 21.2 nM and 1.0 in (**c**)

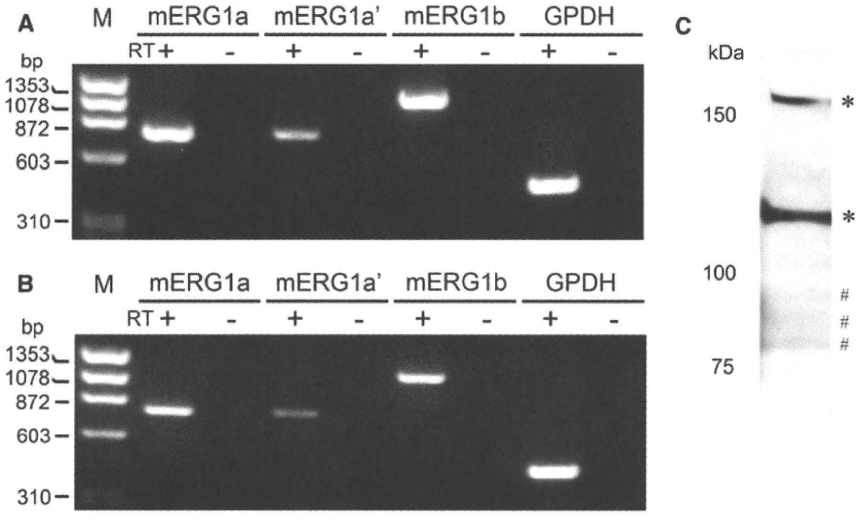

Fig. 9 Expression of mouse ERG1 isoforms in HL-1 cells and mouse atrium. PCR products amplified from cDNA derived from HL-1 cells culture (passage 40) (**a**) and atrial tissues dissected from adult mice (**b**), using primer pairs directed to mERG1a, mERG1a′ or mERG1b. *M* indicates a molecular maker of ϕX174/*Hae*III digest. **c** Western blot of total protein extracts from HL-1 cells (passages 45–47). Blotting with an antibody specific for ERG1 shows two mERG1a glycoform bands (*) at 120 and 160 kDa as well as three mERG1b glycoform bands (#) at 80, 87 and 93 kDa

glycosylated and unglycosylated ERG1a, respectively, in rat and canine ventricular myocytes (Jones et al. 2004), although contamination of signal attributed to ERG1a′ may be possible because of a small difference (~6 kDa) in protein size. On the other hand, we did observe three faint bands with lower molecular mass of 80, 87 and 93 kDa, which are consistent with bands attributed to different glycosylated forms of ERG1b in human and canine ventricular myocytes (Jones et al. 2004) and K562 human leukemic cells (Cavarra et al. 2007).

Recently, gene silencing by RNAi has become a broadly used technology for exploring gene function (Hannon 2002). In the present study, the functional relevance of mERG1 gene expression in HL-1 cells was determined using the RNAi technique. Two siRNA duplex oligonucleotides against all isoforms of mERG1 and ncRNA were

individually transfected into HL-1 cells together with a plasmid vector encoding GFP. Transfection efficacy estimated with green fluorescence was very low (≤5%), which never allowed us to detect an obvious decrease in mERG1 transcripts or proteins at the culture level (data not shown). However, the effects of siRNA were evident in whole-cell membrane current recorded from single GFP-positive cells. Compared to recordings in cells transfected with GFP alone (Fig. 10a), a much smaller time-dependent outward current was observed in cells transfected with siRNA, apparently due to a marked decrease in I_{Kr} amplitude (Fig. 10c, d). The effect of siRNA was attributable to specific knockdown of mERG1 expression because cells transfected with scRNA displayed currents with comparable amplitude to those recorded from cells transfected with GFP alone (Fig. 10b). I_{Kr} density determined by tail current elicited at −50 mV after the 1-s voltage steps to +30 mV was 1.95 ± 0.31 and 1.2 ± 0.34 pA pF^{-1} in cells transfected with siRNA-1 and siRNA-2, respectively. Both values were significantly smaller than those obtained from cells transfected with GFP alone (19.15 ± 2.34 pA pF^{-1}, $P < 0.01$) or with ncRNA (19.00 ± 2.69 pA pF^{-1}, $P < 0.01$) (Fig. 10e).

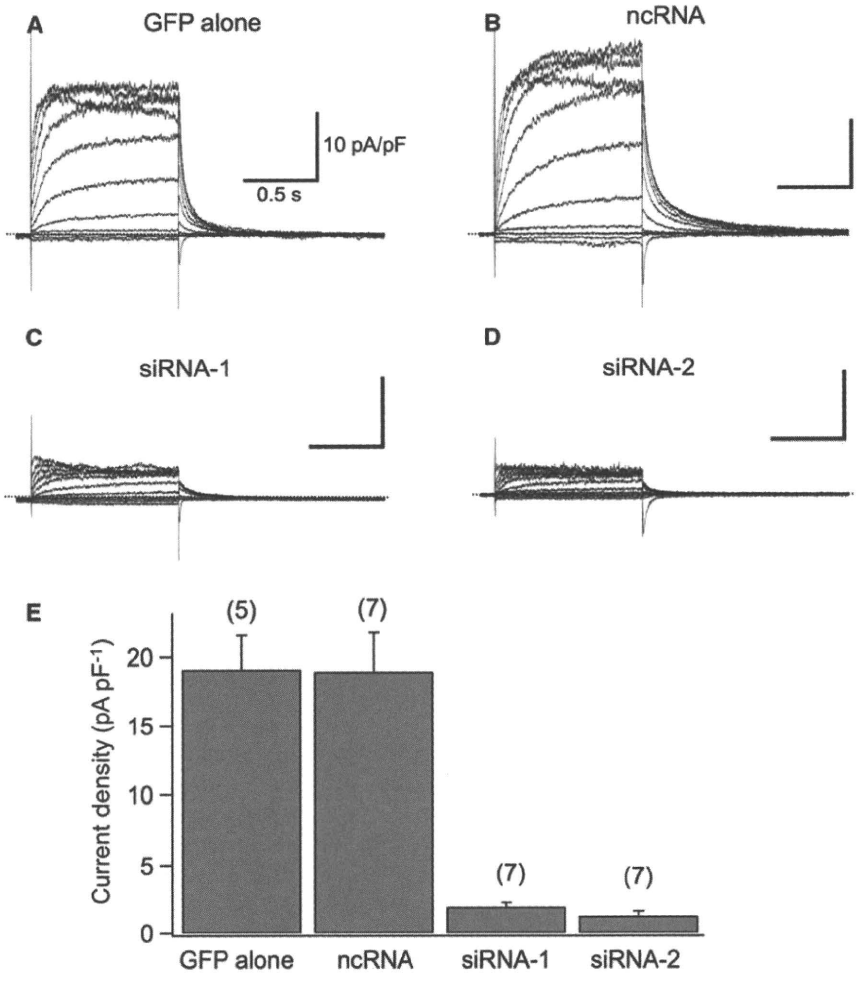

Fig. 10 Knockdown of mouse ERG1 with siRNA in HL-1 cells. Typical current traces recorded from HL-1 cells (passages 40, 41) transfected with GFP alone (**a**), GFP and nonspecific ncRNA (**b**), GFP and siRNA-1 (**c**) and GFP and siRNA-2 (**d**). Cell was held at −50 mV and given 1-s voltage steps to various potentials between −80 mV and +40 mV. **e** Bar graph displaying I_{Kr} density in each group (GFP alone, $n = 5$; GFP plus ncRNA, $n = 7$; GFP plus siRNA-1, $n = 7$; GFP plus siRNA-2, $n = 7$). Tail current was elicited upon repolarization to −50 mV following the 1-s depolarizing steps to +30 mV

Discussion

In this article we describe the basic biophysical properties and molecular identity of I_{Kr} channels in HL-1 cells, the unique murine cardiac cell line established by Claycomb et al. (1998). Our current recordings demonstrated that most of the outward conductance in these cells was dominated by E-4031-sensitive current, which exhibited comparable characteristics to I_{Kr} in native mammalian cardiac cells, i.e., voltage- and time-dependent activation, prominent inward rectification, high K^+ permeability and nanomolar sensitivity to dofetilide or E-4031. In addition, we found that HL-1 cells possessed multiple transcripts and